

Variability in phytoplankton shape dominance in marine pelagic systems: prevalence of different adaptive strategies in the eastern Arabian Sea during the winter monsoon

Pranoy Paul^{1,2}, Jagadish S. Patil*¹ and Arga Chandrashekar Anil¹

1. CSIR-National Institute of Oceanography, Dona Paula 403004, Goa, India.

2. School of Earth, Ocean, and Atmospheric Sciences, Goa University,
Taleigao Plateau, Taleigao 403 206, Goa, India.

*Corresponding: patilj@nio.org

Abstract

Phytoplankton communities from pelagic systems were assessed to explore the potential of using commonly used traits (such as cell geometry and taxa) as ecological function indicators from the data generated during the winter monsoon in the eastern Arabian Sea (AS). Altogether data from two oceanic i.e. convective mixing influenced non-oligotrophic northeastern-AS (NEAS-O and Rossby wave-influenced oligotrophic southeastern-AS (SEAS-O) and one coastal (NEAS-C) cruises were utilized to decipher the ecological inferences. Overall phytoplankton shapes showed a high level of redundancy by selecting only a few dominant shapes (5 of 22 shapes), though taxonomic diversity was rich (164 species). The taxonomic and morphological approach adopted revealed high species and shape diversity in NEAS-O than in high-abundance NEAS-C and low-abundance SEAS-O. Also, the shape diversity and dominant shapes (cylinder, elliptic-prism, and prism-on-parallelogram) remained the same in oceans than NEAS-C where combined (cylinder+2 half-sphere) and simple (elliptic-prism) shapes dominated. Additionally, the Rossby-wave front and its reminiscence in SEAS-O and sea-surface-temperature fronts in NEAS-C favored simple and combine shaped phytoplankton, respectively. The morphological properties assessment revealed that the dominant shapes adapted the strategy to conserve the optimal surface-to-volume ratio (S:V) irrespective of changes in greatest-axial-linear-dimension (GALD) in NEAS-O and SEAS-O but not in NEAS-C. However, the dominant shapes in the NEAS-O and SEAS-O opted for high S:V with low GALD and low S:V with high GALD, respectively, while high S:V with no relation with GALD in NEAS-C suggests the prevalence of different adaptive strategies to cope with the respective hydrographic conditions, particularly nutrient availability.

Key Words: Phytoplankton; Taxonomy; Cell geometry; Northeastern Arabian Sea; Southeastern Arabian Sea; Winter monsoon

Introduction

Phytoplankton, which are vital in ecosystem functioning, food-web dynamics, fisheries, and biogeochemical cycling of essential micro and macronutrients, are not only taxonomically diverse but also show amazing intra- and inter-specific morphological diversity with organisms ranging greatly in the magnitude of size (Finkel et al., 2010) and a wide range of shapes (Hillebrand et al., 1999; Sun & Liu, 2003). Traditionally, the morphological attributes are being used only for taxonomic studies but it does not reflect the ecological functions (Salmaso & Padisak, 2007; Naselli-Flores et al., 2007). Lewis (1976) first noted the ecological value of morphological descriptors in phytoplankton resource acquisition (light and nutrient uptake) under the pressure of natural selection and competition. The adaptive value of the morphological variability and differences in morphology adopted for diverse ecological strategies by phytoplankton was studied by Margalef (1978) and later explored by Reynolds (1997). Few shapes are best adapted to certain environmental conditions than others so the phytoplankton with such shapes should have better fitness and diversity (Ryabov et al., 2021). The aquatic ecosystem's ecological state can be assessed by understanding the adaptive value of different phytoplankton morphologies therefore, morphological diversity can be considered a key factor allowing a particular ecological group to withstand the various environmental conditions experienced in the ecosystem (Naselli-Flores, 2014).

The trait-based approaches in phytoplankton ecology have become common and such approaches have the potential to increase our insight into the organization of ecological communities and predict their reorganization under any environmental change (Litchman & Klausmeier, 2008). This is because phytoplankton are relatively simple and have well-defined traits that determine their ecological niche (Litchman & Klausmeier, 2008). The well-defined commonly used traits in phytoplankton can be classified into three categories (Litchman & Klausmeier, 2008; Weithoff & Beisner, 2019), i) Morphological: size, shape, greatest axial linear dimension (GALD), biovolume, mucilage presence/absence, biological form (unicellular/colonial/filament/chains), ii) Physiological: presence/absence of silica demand, heterocysts (N₂-fixation), mixotrophy, toxin production, resting stages, dominant pigment type, nutrient and/or light uptake parameters and iii) Behavioral: presence/absence of flagella, aerotypes. Among all the above-mentioned traits, morphometric traits like size and shape are considered master traits (Weithoff & Beisner, 2019) which affect nutrient acquisition, sinking, and grazer susceptibility (Grover, 1989; Smayda, 1970; Thingstad et al., 2005). Size and shape are also plastic in nature and depend on many environmental variables, such as light levels, nutrient concentrations, and grazing pressure (Chisholm, 1992; Duarte et al., 1990).

Further, in trait-based studies, species sharing similar adaptive traits are grouped even if they are taxonomically distinct (Simberloff & Dayan, 1991). From the phytoplankton viewpoint, the pelagic habitat and its main representative phyla and their ecology are relatively similar across both marine and freshwater ecosystems (Weithoff & Beisner, 2019). Despite such similarity, the focus of research differed between systems i.e., the majority of research in the marine considered how traits and trait distribution derive processes that determine the environmental conditions (like biogeochemistry) but it is the opposite in the freshwater where the focus is on how communities respond to the environment and which environmental factors drive the trait-based community assembly (Weithoff & Beisner, 2019). For instance, the increasing uses of trait-based studies to explain and understand phytoplankton community is limited to distribution (Kruk et al., 2010), seasonal dynamics (Salmaso & Padisak, 2007), diversity, and community structure (Litchman & Klausmeier, 2008) in freshwater, whereas in the marine ecosystem, the studies are limited to spatiotemporal variation (Stanca et al., 2013), biogeographic trait patterns (Barton et al., 2013), biogeochemical processes such as primary production and nitrogen fixation (Breton et al., 2017), oceanic biogeochemistry (Litchman et al., 2007,2015; Finkel et al., 2010) and phytoplankton dynamics (Alexander et al., 2015). Many morphological traits might be strategic and help in explaining phytoplankton differences and patterns under contrasting hydrodynamic conditions (Fraisse et al., 2013). Thus morphological traits play a pivotal role in the determination of phytoplankton ecological niches (Aubry et al., 2017). The morphological adaptive strategy that results in response to environmental changes helps differently-sized phytoplankton organisms to coexist making it like a geometric concurrence (Segura et al., 2013; Roselli & Basset, 2015). However, to our knowledge, the information on the variations in phytoplankton shapes concerning different hydrographic settings in the marine pelagic systems is not available and was addressed in the present study by selecting the eastern Arabian Sea in the Northern India Ocean, a well-studied system, as a reference. A similar approach was attempted to study the rock-pool micro-phytoplankton community from the intertidal zone (Paul et al., 2021) but studies from the open ocean are limited even though there exist few datasets on cell volumes (Chitari & Anil, 2017).

The Arabian Sea (AS) is considered one of the unique oceanic basins owing to its high productive periods in winter (WM) and summer monsoon (SM) caused by the seasonal reversal of wind direction and associated drastic changes in the surface currents (Banse, 1987) and the data presented here corresponds to winter monsoon from eastern AS (EAS). The physical change in the water column associated with the reversal of monsoonal winds governs the productivity of the Arabian Sea (Wiggert et al., 2005). During WM, the hydrographic conditions in the northern and

southern regions of EAS are significantly different i.e. currents bring in high nutrients through convective mixing in the NEAS which supports phytoplankton production (including bloom; Banse, 1987; Sarma et al., 2019) and was also noticed in this study i.e. higher in NEAS (both open and coastal) than SEAS-O (Supplementary Table 1 and 2). The convective mixing in NEAS is triggered by the cold-dry north-easterly continental wind blowing over the surface waters causing evaporation (Madhupratap, et al., 1996; Weiler et al., 2002). The convective mixing during winter monsoons deepens the mixed layer depth (MLD) and enhances nutrient availability (Sawant & Madhupratap, 1996). Whereas in SEAS, WM is defined by the existence of seasonal down-welling Rossby waves (Shankar et al., 2002) which, along with its associated currents brings the nutrient-enriched low saline water mass from the western boundary of the Bay of Bengal (Shenoi et al., 2002) and triggers primary producers (Kumar et al., 2004, Amol 2018) in the otherwise warmer oligotrophic waters (Vijayan et al., 2021). Additionally, the mesoscale features such as sea surface temperature (SST) fronts supporting rich phytoplankton biomass than the adjoining non-fronts are also prevalent in AS. However, more SST fronts are reported in NEAS than in SEAS (Kurian et al., 2020). Therefore, in the present study, an attempt has been made to understand the distribution of phytoplankton shapes and species composition between contrasting hydrographic settings such as (a) nutrient-rich coastal and open ocean systems, (b) oligotrophic and non-oligotrophic ocean systems, and (c) SST fronts and non-fronts from both coastal and ocean ecosystems. Through this study, an attempt is made to explore the possibility of using phytoplankton shapes (>5 microns) as ecological function indicators in marine pelagic systems.

Methodology

Study area and sampling strategies

The present study was carried out in the north (NEAS) and the south (SEAS) EAS during the winter monsoon of 2015-16. In the NEAS, two cruises, *R/V Sindhu Sankalp* (11-22 February 2015) in the open ocean (NEAS-O) and *R/V Sindhu Sadhana* (18 November- 2 December 2016) in the coastal (NEAS-C) were taken during late winter monsoon and early winter monsoon, respectively and another cruise, *R/V Sindhu Sadhana* (6-17 November 2016) was taken in the open ocean of SEAS (SEAS-O) during early winter monsoon (Fig. 1 and Supplementary Fig. 1). The water samples from NEAS-O (20 stations), NEAS-C (38 stations), and SEAS-O (31 stations) were collected at discrete depths (surface to 100m) with 10 L Niskin bottles attached to 32 Carousel Water Sampler (Sea-bird Electronics Inc.; SBE) which is operated with the SBE 911 plus CTD for real-time data acquisition. The hydrographic data revealed that in NEAS the surface and sub-surface waters are more saline and are relatively cooler and warmer, respectively than SEAS (Fig. 2). Also, the fluorescence and

nutrient concentrations are relatively higher in NEAS than in SEAS. Additionally, differences in frontal and non-frontal regions were also observed. Most of the hydro-graphic data are published in detail elsewhere (see Bernal et al 2018 and Sarma et al 2019 for more details) and here only a summary of the same is presented in Supplementary Tables 1 and 2.

Phytoplankton sample collection and analysis

A fixed volume (1L) of the water sample was preserved with 4% Lugol's iodine and used for further analysis. An aliquot (2-5 ml) of the sample volume in duplicate was analyzed from the concentrated (by sedimentation (48h) and siphoning technique) 100ml using an inverted microscope (IX-73 Olympus Make) to access the phytoplankton composition and abundance. The taxonomic identification of phytoplankton was carried out based on standard identification keys (Tomas 1997; Taylor, 1973).

The morphological measurements (Length, width, breadth, area, volume, and maximum linear dimension) for each phytoplankton cell or colony were performed using a factory-calibrated FlowCAM (Fluid Imaging Technologies) at 4x magnification (flowcell 300 μm) and a microscope digital camera adapter system (QimagingMicroPublisher 5.0 RTV) attached to the inverted microscope at 200x-600x magnification (Olympus IX73), respectively. These measurements were then used for the calculation of volume (V ; μm^3) and surface area (S ; μm^2) following Hillebrand et al., (1999) and Sun and Liu (2003). In algal ecology and physiology, shape and size variability plays a key role (Capblancq & Catalan, 1994) wherein the surface/volume ratios of a biomass unit need to be maintained within physiologically necessary bounds in a given environment (Lewis, 1976). Given this, the surface-to-volume ratio ($S:V, \mu\text{m}^1$) of the phytoplankton was calculated according to Lewis (1976) and Aubry et al., (2017). For chain-forming cells like *Chaetoceros* and *Skeletonema*, each cell in the chain was considered and the morphological measurements were taken in higher magnifications (400x or 600x). The greatest axial linear dimension (GALD; μm) or maximum linear dimension (MLD) (Weithoff & Beisner, 2019) is measured directly from the linear dimensions like diameter, height, total length, apical axis length of a given cell based on the geometric approximation given by Hillebrand et al., 1999 and Sun et al., 2003. Here in this study, the GALD of a cell is measured according to its cell geometry as described by Ryabov et al., 2021. For instance, in the simple shapes the maximum cell linear dimension (e.g. diameter in the sphere, height in ellipsoid and cylinder, apical axis length in prism on parallelogram, etc.) was considered as GALD whereas, for combined shapes (Box+2 Cylinders, Cylinder+2 Half spheres, Ellipsoid+2 Cones+Cylinder, etc.) consisting of few segments measured separately (e.g. cylinder with 2 half spheres), the sum of the linear dimensions of these parts or the total height or length were considered.

Overall, a total of 22 shapes were identified among which 11 shapes were simple (Box-B, Cone-C, Cylinder-Cyl, Cymbelloid-Cym, Ellipsoid-Elli, Elliptic prism-ElliP, Half sphere-Hs, Prism on parallelogram-PoP and Prism on triangle-PoT, Prolate spheroid-Ps, and Sphere-S) and 8 were combined (Box+2 Cylinders-B2Cyl, Box+Elliptic prism-BElliP, Cone+Half sphere-CHs, Cylinder+2 Half spheres-Cyl2Hs, Ellipsoid+2 Cones+Cylinder-Elli2CCyl), Elliptic prism+4 Cones-ElliP4C, Prolate spheroid+2 Cylinders-Ps2Cyl, and 2 Cones-2C). Among them, the 3 shapes with their girdle view (e.g. Cyl, PoP, PoT) are considered equivalent to their original shape as the geometric formula was the approximation of the original shape.

Data analysis

Univariate measures such as species count, Abundance, Shannon–Wiener’s diversity, species richness, and evenness were performed on log-transformed species and shape data. The clustering of frontal and non-frontal phytoplankton was performed through the Bray–Curtis similarity and group average methods. For the analysis, log (x+1) transformed species and shape data were used, and the grouping was done at a 50% level to find the significant similarities. Further, the log-transformed taxa and shape data were subjected to a two-way analysis of variance (ANOVA) to evaluate the variation between regions as well as between the frontal and non-frontal regions. The relationship between the greatest axial linear dimension (GALD) and S:V was determined by using linear regression on log(x+1) transformed data. The significance level was set at $p < 0.05$ and the determination coefficient (R^2) was considered as the proportion of variation in S:V which can attribute to GALD, whereas the slope (b) showed the degree to which the S:V would vary as GALD increases. If the slope (b) value is very low, for instance, $b = -0.06$ for PoP, that means a decrease in S:V of $0.06 \mu\text{m}^{-1}$ for each μm increase in GALD. The negative correlation between GALD and S:V in general means that as the GALD increases the S:V decreases, and vice versa. Univariate measures calculation and clustering analysis were performed using statistical software PRIMER 6, ANOVA was performed using Statistica software (release 8), linear regression analysis and box plots were plotted using R program (R core Team 2020) and ODV plots were plotted using Ocean Data View 4 (Schlitzer, 2015).

Results

Taxonomic and shape diversity of the North-eastern Arabian Sea (NEAS)

A total of 133 (belonging to 63 genera) and 83 (belonging to 48 genera) species were recorded in the open ocean (NEAS-O) and coastal (NEAS-C) regions, respectively (Supplementary Table 3). In NEAS-O diatoms (81%) comprising 54 species (36 centric and 18 pennate species) followed by

dinoflagellates (19%) comprising 89 species dominated the community whereas, in NEAS-C, diatoms (94%) comprising 44 species (30 centric and 14 pennate species) followed by dinoflagellates (6%) comprising 39 species dominated the phytoplankton community. Despite diatom dominance, the contribution to the total community was higher in the open ocean (82-98%) than in the coastal (77%) (Fig. 3). ANOVA revealed significant differences in phytoplankton community structure and species dominance between the open ocean and coastal region ($p=0.003$). The diversity analysis reveals that the species count, richness, evenness, and diversity were higher in the NEAS-O than in NEAS-C except for the abundance which showed an opposite trend for both taxonomy and shape (Fig. 4a-j).

In the NEAS-O, centric diatoms *Rhizosolenia styliformis* and *Probosica alata* of Cyl shape followed by pennate diatoms *Lioloma* sp. of B shape and *Navicula* spp. of ElliP shape and dinoflagellate species *Protoperidinium* spp of 2C shape were the major contributors. Whereas in NEAS-C, centric diatom *Skeletonema* sp. of Cyl2Hs shape and *Leptocylindrus* sp. of Cyl shape followed by pennate diatom *Pseudonitzschia* spp. of PoP shape and *Thalassionema nitzschoides* of B shape and dinoflagellate species *Protoperidinium* spp. of 2C shape dominated the community. It is notably interesting that despite the overall phytoplankton community was diatom dominated; the community structure was quite different within diatoms except for the dinoflagellates.

All the recorded phytoplankton species are categorized into a total of 19 (11 simple and 8 combined) and 16 (11 simple and 5 combined) morphometric shapes from NEAS-O and NEAS-C, respectively. Simple-shaped (88%) phytoplankton dominated in NEAS-O whereas, combined-shaped (55%) in NEAS-C. Among the simple shapes, Cyl (54%) was the dominant shape followed by ElliP (9%), B (9%), Elli (6%), and ElliP4Cs (5%) in NEAS-O. Maximum species diversity was observed in Elli2CCyl representing 36 phytoplankton species (all dinoflagellates) followed by Cyl with 27 species (22 centric diatoms and 5 dinoflagellates), Elli with 20 species (all dinoflagellate) and ElliP with 16 species (11 centric and 5 pennate diatoms). Among the combined shaped phytoplankton, Cyl2Hs (53%) was dominant followed by PoP (12%), ElliP (12%), and Cyl (12%) in NEAS-C. The maximum species diversity was observed in Cyl with 17 species (all centric diatoms) followed by ElliP with 14 species (11 centric and 3 pennate diatoms) and Elli with 14 species (all dinoflagellates).

The linear regression analysis of dominant phytoplankton shapes (abundance $\geq 60\%$) from NEAS-O revealed a significant negative correlation between GALD and S:V ($p < 0.05$), whereas, no significant correlation was observed for NEAS-C (Fig. 8). In the NEAS-O, the determination of coefficient (R^2) for dominant shapes showed low values. However, in the present study, the

dominant shapes (Cyl, ElliP, and PoP) of both coastal and open ocean ecosystems in NEAS adopted high S:V with a low GALD strategy. The results point out that all the dominant shapes in NEAS-O are attenuated (Cyl, ElliP, and PoP) and have adapted the strategy to conserve the optimal S:V which changes very minimally as the GALD increases (Fig. 8).

Additionally, the sampling at 38 stations in the NEAS-C region encompasses both frontal and non-frontal regions and are categorized and presented accordingly as follows: a) East front (EF) comprising 7 stations, b) West front (WF) comprising 5 stations, c) Main front (MF) comprising 18 stations and d) Non-front (NF) comprising of 8 stations (Figure S1). It is evident from the comparative community and diversity analysis that the frontal waters showed high abundance and species composition compared to the non-frontal waters (Fig. 5a-e). Among all the stations, MF recorded the maximum number of phytoplankton species followed by EF, NF, and WF waters. The phytoplankton abundance was higher in all the frontal stations compared to NF. Interestingly, species richness, evenness, and diversity were higher in the NF stations compared to all the frontal stations (MF, WF, and WF) (Fig. 5c-f). A total of 67 phytoplankton species (39 diatoms (26 centric and 13 pennate) and 28 dinoflagellate species) representing 44 genera were recorded in the MF followed by EF with 52 species (32 diatoms (20 centric and 12 pennate) and 20 dinoflagellate species) from 38 genera, NF 50 species (27 diatom (18 centric and 9 pennate) and 23 dinoflagellate species) from 34 genera and WF 49 species (31 diatom (19 centric and 12 pennate) and 18 dinoflagellate species) from 36 genera. Diatoms in the frontal waters contributing 90-98% of the total abundance dominated the entire phytoplankton community whereas dinoflagellates contributed only 2-10%. The non-frontal waters were also diatom-dominated contributing 81% of the total abundance and the remaining 19% were contributed by dinoflagellates.

The shape-based morphometric analysis from the frontal and non-frontal regions of NEAS-C reveals that simple shapes dominated the WF (56%) and NF (69%) whereas, combined shapes dominated the EF (57%) and MF (55%). The dominant shape in all the frontal regions (EF, WF, and MF) were Cyl2Hs (43-56%) followed by PoP (11-15%), ElliP (11-12%), and Cyl (11-15%). The dominant shape in the NF region was Cyl (23%) followed by Cyl2Hs (22%), PoP (17%), and ElliP (15%). The maximum shape diversity in all the frontal (11-14 species) and non-frontal (13 species) regions were observed in the Cyl shape. However, the univariate measurement reveals that the shape richness, evenness, and diversity were higher in the non-frontal regions than in the frontal regions except for the abundance (N) which was higher in the frontal region (Fig. 5f-j).

The dominant shapes such as Cyl2Hs (centric diatom *Skeletonema* sp.), PoP (*Pseudonitzschia* spp.), ElliP (*Chaetoceros* spp. and *Navicula* spp), and Cyl (*Thalassiosira* spp. and *Leptrocylindrus*

spp.) in the frontal region is represented by diatoms. In the non-frontal region, Cyl was the dominant shape and is majorly represented by *Leptocylindrus* spp. and *Thalassiosira* spp. Taxonomically, the centric diatom community was dominated by *Skeletonema* sp. and *Leptocylindrus* spp. whereas; the pennate community was dominated by *Pseudonitzschia* spp. and *Navicula* spp. The dinoflagellate communities in both frontal and non-frontal waters were dominated by *Protoperidinium* spp. The cluster analysis for both taxonomy and shape shows two distinct clusters in which all the frontal stations (MF, WF, and WF) showed significant taxonomic similarity and formed one single cluster and NF as another cluster (Supplementary Figure 4) however the number of shapes was insignificant between the frontal and non-frontal regions. ANOVA also revealed significant ($p=0.0001$) taxonomic differences between MF and NF regions but significant shape dissimilarity between frontal and non-frontal regions was not found ($p>0.05$).

Taxonomic and shape diversity of the South-eastern Arabian Sea (SEAS)

A total of 74 phytoplankton species belonging to 35 genera were recorded from two transects (T1 and T2) in SEAS-O. Of the 74 species, 30 and 44 species were represented by diatoms (21 centric & 9 pennate species) and dinoflagellates respectively despite the high number of dinoflagellate species, the phytoplankton community was dominated by diatoms (77%). Unlike NEAS-O, the percentage contribution revealed the maximum contribution by pennate diatoms (48%) followed by centric diatoms (29%) and dinoflagellates (23%). The centric diatom community was dominated by *Cerataulina* sp. and *Chaetoceros* spp. whereas; *Pseudonitzschia* spp. and *Thalassiothrix* sp. dominated the pennate diatom community. The dinoflagellate community was dominated by *Gyrodinium* sp., *Protoperidinium* spp., and *Scrippsiella* sp. Between the transects, transect 1 (T1) comprising 19 stations showed a slightly higher abundance compared to transect 2 (T2) comprising 12 stations. A total of 68 species belonging to 35 genera and 42 species belonging to 28 genera were recorded from T1 and T2 respectively. Of the 68 species in T1, 28 and 40 species were represented by diatoms (19 centric and 9 pennate species) and dinoflagellate respectively. Whereas in T2 they were represented by an equal number of species i.e. 21 species of diatom (13 centric and 8 pennate species) and dinoflagellates. In both the transect, diatoms (76% in T1 and 84% in T2) dominated the community followed by dinoflagellates (24% in T1 and 16% in T2). Among the diatoms, the pennate contribution was higher than centric diatoms. Also, the community in both transects is presented by the same dominant species. For instance, In T1, the centric diatom community was dominated by *Cerataulina* sp., *Chaetoceros* spp., and *Thalassiosira* sp. whereas, *Pseudonitzschia* spp. and *Navicula* sp. dominated among pennate diatoms. The dinoflagellate community was dominated by *Protoperidinium* sp., *Gyrodinium* sp., and *Scrippsiella* sp. In T2, *Chaetoceros* spp. and

Thalassiosira sp. were the dominant centric diatoms whereas; *Pseudonitzschia* sp. and *Thalasiothrix* sp. dominated the pennate diatom community. *Gyrodinium* spp. and *Protoperidinium* spp. dominated the dinoflagellate community. Univariate measures revealed that T1 showed higher species number, abundance, richness, diversity, and evenness than T2 (Supplementary Fig. 2a-e).

All the recorded 74 phytoplankton species are categorized into 12 morphometric shapes (9 simple and 3 combined) were recorded in the SEAS-O. Simple shapes showed maximum contribution (93-97%) compared to the combined shapes (3-7%). Considering the T1 and T2 transect, Cyl (23%) followed by PoP (19%), ElliP (18%), Elli, and B (14% each) dominated the phytoplankton community. Both the T1 and T2 recorded a similar number of shapes but Cyl (29%) dominate the former and PoP (32%) in the latter. ElliP2CCyl and Cyl showed maximum diversity representing 16 species each in T1 and Cyl (9 species) and Elli (7 species) in T2 showed the maximum diversity. The most dominant shape (Cyl) in T1 was represented by centric diatoms *Cerataulina* spp. and *Thalassiosira* spp. and the dominant shape in (PoP) T2 was represented by pennate diatom *Pseudonitzschia* spp. The diversity analysis of T1 and T2 revealed that shape abundance, evenness, and diversity were higher in T1 except for richness (d) which was higher in T2 (Supplementary Fig. 2f-j). Similar to NEAS-O, the linear regression analysis of dominant phytoplankton shapes (abundance $\geq 60\%$) revealed a significant negative correlation between GALD and S:V ($p < 0.05$) (Fig. 8) with the highest determination of coefficient (R^2) was recorded for PoP followed by Cyl. The dominant shapes (Cyl, ElliP, and PoP) of SEAS-O adopted low S:V with a high GALD strategy. The results point out that all the dominant shapes in SEAS-O are attenuated (Cyl, ElliP, and PoP) and have adapted the strategy to conserve the optimal S:V which changes very minimally as the GALD increases (Fig. 8).

Additionally, T1 in SEAS-O encompasses 19 stations in both frontal (F) and non-frontal (NF) regions and the results are presented accordingly. Of the 19 stations, 10 stations were frontal (F) and 9 stations were non-frontal (NF). Further, the NF region was again divided into two zones NF-west (NFW) and NF-east (NFE). The diversity analysis shows that the species count, richness, evenness, and diversity are higher in the frontal region than in the NF regions except for the abundance which is higher in the NFE (Fig. 6a-e). A total of 45 species belonging to 24 genera and 38 belonging to 27 (in NFW) and 26 (in NFE) genera were recorded in F and NF, respectively. Of the 45, 18 and 27 species correspond to diatoms (13 centric and 5 pennate species) and dinoflagellates, respectively in F whereas in NF, 20 diatoms (12 centric and 8 pennate species) plus 18 dinoflagellates and 16 diatoms (10 centric and 6 pennate species) plus 22 dinoflagellates were recorded from NFW and NFE respectively. In all the regions diatoms dominated the phytoplankton community i.e. 70%, 79%,

and 77% in frontal, NFW, and NFE, respectively. In the frontal region, pennate diatom (*Pseudonitzschia* spp.) dominated whereas, centric diatoms (*Chaetoceros* spp. and *Cerataulina* sp.) dominated the NF (NFE and NFW) regions. The dinoflagellate community was dominated by *Gyrodinium* sp. and *Protoperidinium* spp. in both frontal and NF regions. The cluster analysis shows that frontal and NFE are significantly similar and form a single cluster in the dendrogram (Supplementary Fig. 3).

Between non-frontal (both NFW and NFE) and frontal, a total of 11 and 10 morphometric shapes were recorded in the former and later, respectively. Simple-shaped phytoplankton dominated (92-95%) both the frontal and non-frontal regions whereas combined shape contributed only 5-8%. Among the simple shapes, Cyl-shaped phytoplankton dominated (28-41%) the non-frontal regions whereas frontal regions were co-dominated by Elli (26%) and Cyl (21%) shape (Fig. 7). Interestingly the species structure was different despite Cyl-shape was most dominant in both the frontal and non-frontal regions. In NFW Cyl-shape was represented by *P. alata* and *Cerataulina* spp. and NFE was dominated only by *Cerataulina* spp. The Elli-shape was mostly represented by dinoflagellates (*Gyrodinium* spp. and *Scrippsiella* spp.) in the frontal regions. Maximum diversity among shapes in the frontal regions was observed with Cyl, Elli, and ElliP2CCyl, which were represented by 11 species each. Whereas, maximum species diversity among the non-frontal regions was observed with Cyl (7-10 species) and Elli (7-9 species) shapes. The diversity analysis reveals that NFE and NFW have a similar number of shapes and richness is relatively higher than in the frontal regions (Fig. 6 f & d). NFE showed the maximum abundance followed by front and NFW. The cluster analysis showed the non-frontal regions are similar to each other but dissimilar to the frontal regions but ANOVA does not show any significant dissimilarity ($p > 0.05$) (Supplementary Fig. 3).

Taxonomic and shape diversity comparison between NEAS-O and SEAS-O

The chain-forming centric diatoms (e.g. *P. alata* and *R. styliformis*; 62%) dominated the NEAS-O whereas pennate diatoms (*Pseudonitzschia* spp.; 48%) dominated in the SEAS-O. The percentage contribution of diatom and dinoflagellates were different in the NEAS-O and SEAS-O where dinoflagellates contributed less (2%) in the former than the latter (23%). The dinoflagellate community was dominated by a single genus (*Protoperidinium* spp.) in NEAS-O whereas *Gyrodinium* spp., *Protoperidinium* spp., and *Scrippsiella* spp. co-dominated the community in the SEAS-O. The abundance, species richness, evenness, and diversity were higher in the NEAS-O than in SEAS-O (Fig. 4a-e). The cluster analysis based on Bray-Curtis similarity shows the NEAS-O and SEAS-O are significantly dissimilar (Supplementary Fig. 5). The shape richness was higher in NEAS-O (19 shapes) than in SEAS-O (12 shapes) (Fig. 4f-j). The most dominant shape was Cyl

comprising 27 phytoplankton species (22 centric diatoms and 5 dinoflagellate species) and PoP comprising 3 pennate diatom species in NEAS-O and SEAS-O, respectively (Supplementary Fig. 6). The most species diverse shape Elli2CCyl comprised 36 and 16 dinoflagellate species in NEAS-O and SEAS-O, respectively. The univariate analysis revealed that the number of shapes, abundance, and shape richness was higher in NEAS-O compared to SEAS-O but shape evenness and diversity showed an opposite trend (Fig. 4f-j).

Discussion

This study recorded 164 species and represents most (accounting for up to 71%) of the geometric shapes (22 out of 31 described shapes of Sun & Liu (2003)) described for phytoplankton in literature (Supplementary Table 3). The remaining unrecorded 9 shapes are mostly represented by the freshwater species or the phytobenthos in the sunlit zone or belong to groups (e.g. flagellates, Euglenophyceae, Chlorophyceae) that were not recorded due to known technical limitations (e.g. preservatives) through microscopy approach. Amongst them, the latter may be of significance as the present study is dealing with species from marine pelagic systems but not from freshwater or benthic habitat. The phytoplankton marker pigment data for the eastern Arabian Sea, including from the presented NEAS-O transect (Sarma et al. 2018) and available literature (Roy et al., 2015; Chandrasekhararao et al., 2018; Bemal et al., 2019) indicated the presence of groups such as non-thecate dinoflagellates (peridinin), Chrysophyceae (19'-butanoyloxyfucoxanthin), haptophytes (19'-Hexanoyloxyfucoxanthin), cyanobacteria (Zeaxanthin), *Prochlorococcus* (divinyl chlorophyll a and b), chlorophytes (chl b), and prasinophytes (prasinoxanthin). Since the present study is based on microscopic analysis, only the dominant groups (> 5 µm) like diatoms and thecate dinoflagellates are possible to consider but not the above-mentioned groups (except picophytoplankton due to methodological limitations (Lugols-Iodine and Formalin; Williams et al., 2016). Also, picophytoplankton are not considered and *Trichodesmium* though preserved well with the fixative but was not found in this study. Considering methodological limitations in the microscopic method, the phytoplankton shape data are generally underestimated, and even then they are successfully used and tested to understand the phytoplankton dynamics in both freshwater (mostly community-related) and marine systems (process-related) (e.g. Stanca et al., 2013; Aubry et al., 2017). Despite methodological limitations, this study also revealed that EAS harbors most of the described phytoplankton shapes and species showing dissimilar spatial distribution patterns concerning abundance, composition, and diversity. In this study, the variability in distribution patterns between bioregions having distinct hydrographic conditions is discussed in the subsequent sections.

Variability between Coastal and Open Ocean ecosystems

The contrast in the oceanographic conditions is well reflected in both taxa and morphology for the NEAS-C and NEAS-O phytoplankton communities. The diatom dominance (also reported in previous studies eg. by Vijayan et al., 2021 and references therein) is represented by different species and morphotypes but NEAS-O harbored rich species and shape diversity compared to the NEAS-C. Such high variability in geometric shape is not a coincidence but a morphological adaptation to environmental conditions. Similar findings are also reported from the coastal waters of the Salento Peninsula (Italy) where the phytoplankton shapes were dependent on environmental conditions and strongly varied with the season (Stanca et al., 2013). The winter convective mixing and advection induced the availability of high nitrate and phosphate concentration (Sarma et al., 2018; Bemal et al., 2018) favored high species and shape variability in the NEAS. Further, the Rhizosolenoid diatom devoid of nitrogen-fixing endosymbionts (*Richelia*) also signifies nitrate availability (Padmakumar et al., 2010). Amongst the recorded phytoplankton morphotypes, species with Cyl and Cyl2Hs dominated the NEAS-O and co-dominated the NEAS-C, where the chain-forming (*Skeletonema* sp. and *Leptocylindrus* spp.) and non-chain forming (*Rhizosolenoid*) centric diatoms dominated in NEAS-C and NEAS-O respectively, showing spatial variations. In NEAS-C, the Cyl2Hs-shape (solely represented by *Skeletonema*) contributed more than half (53%) of the shape diversity. However, its distribution was restricted only to the upper water column (40m <) (Supplementary Fig. 6) suggesting that Cyl2Hs-shape is the best fit only in the shallow waters or might have had a very strong mechanism to remain afloat in the sunlit zone to exploit the available resources (Smayda & Boleyn, 1966; Durante et al., 2019). For instance, in *Skeletonema*, a high S:V ratio (0.8; Smayda & Boleyn, 1966) and large colony formation are the key features to reducing the sinking rate. In general, the sinking rate is lower in elongated shapes (like Cyl, Cyl2Hs) than in spherical shapes (Durante et al., 2019). Whereas, in the open ocean, the presence of apical process in Cyl-shape i.e. *Rhizosolenia* sp. (as also shown in *Rhizosolenia setiger* by Smayda and Boleyn, 1966) might have helped in reducing the sinking rate. Another experimental study also demonstrates that the spine aid in reducing the sinking rate (Padisak et al., 2003). The dominant (48%) Cyl-shaped diatom in NEAS-O was found to be evenly distributed throughout the water column (Supplementary Fig. 6), making it a successful and best-adapted shape among all the 19 shapes reported. The success of Cyl-shaped phytoplankton can also be inferred by its morphometric traits and adaptive strategies like conserving optimum S:V and high S:V with low GALD, respectively. The regression analysis revealed that the Cyl-shape showed a negative correlation between GALD and S:V with a very low slope ($b=0.131$) value. This means a decrease in S:V of $0.131 \mu\text{m}^{-1}$ for each μm increase in GALD, pointing out that

the dominant shape in the NEAS-O ecosystem was attenuated and has adapted the strategy to conserve the optimal S:V which changes very minimally as the GALD increases.

Variability in contrasting oceanographic settings

Our study finds that both the taxonomic and shape diversity of phytoplankton was higher in the productive non-oligotrophic NEAS-O compared to the non-productive oligotrophic SEAS-O. Cyl-shaped centric diatoms dominated and co-dominated in NEAS-O and SEAS-O, respectively. However, the species representing Cyl-shape are different but were mostly dominated by centric diatoms. In NEAS-O Rhizosolenoid (like *P. alata* and *R. styliformis*) diatoms dominated whereas in SEAS-O *Cerataulina* sp., *P. alata*, and *Thalassiosira* sp. co-dominated with elliptic prism-shaped (*Chaetoceros* spp.) diatoms. *Cerataulina* spp. representing the Cyl-shape is well known for its bloom formation in nutrient-depleted turbulent waters (Ault et al., 2000; Lauria et al., 1999). Such spatial variability in morphotype dominance can be attributable to the prevalence of different hydrographic conditions in NEAS-O (biochemical changes driven by winter convective mixing) and SEAS-O (oligotrophic conditions). The oligotrophic conditions in the SEAS-O have resulted in the low abundance and chain-forming small pennate diatoms, which are known to have advantages over large phytoplankton cells under nutrient-limited conditions making them dominant (Finkel, 2007; Grover, 1989). The oligotrophic condition of SEAS-O is also revealed by the increased percentage contribution of dinoflagellate species (23%) known to be better adapted in nutrient-limited conditions and use their flagella in exploiting a stratified water column. Among the 12 shapes, simple and attenuated shapes like Cyl (23%), PoP (19%), and ElliP (18%) dominated the phytoplankton communities. The less shape diversity reflects the prevailing environmental conditions (oligotrophic waters), which could not afford to support the variety of other shapes, and only the best-adapted shapes flourished. However, it is interesting to note that even if the NEAS-O and SEAS-O showed very different hydrographical conditions and diversity, the shape dominance remained the same: simple attenuated shapes like Cyl or ElliP dominated across this vast gradient. All the dominant shapes have adopted the strategy of conserving their optimum S:V by showing negative correlation and minimal variations as the linear dimension changes (Fig. 8). Moreover, the adaptive strategies opted by the dominant shapes (Cyl, ElliP, and PoP) in NEAS-O and SEAS-O varied. In the NEAS-O, the dominant shapes (Cyl, ElliP, and PoP) opted for high S:V with low GALD, but the dominant shapes in SEAS-O opted for the opposite. Such consistency in morphological traits composition compared to species composition is also reported in various studies (Naselli-Flores & Barone, 2007; Weithoff & Gaedke, 2017; Salmaso & Padisak, 2007), pointing out the importance of trait-based studies. Therefore, it can be said that the phytoplankton cell geometry

or shape in the eastern Arabian Sea (NEAS-O and SEAS-O) showed a high level of redundancy. Redundancy, in this case, means that even if the taxonomic diversity was high, only a small number of shapes dominated. The trait-based studies allow the quantitative assessment of community or ecosystem resistance or resilience to changes through functional redundancy (Lavorel & Garnier, 2002; McGill et al., 2006) which in turn can increase the predictability of future ecosystem function projections than the species-centered taxonomic approaches (Levine, 2016; Martini et al., 2021). Further, the eastern Arabian Sea (NEAS-O and SEAS-O) is well known for the occurrence of large-scale phytoplankton blooms (D'Silva et al., 2012), and the species causing blooms are generally characterized by simple shapes. For example, spherical-shape *Noctiluca* bloom (Sarma et al., 2019; Gomes et al., 2008) and Cyl-shape *Trichodesmium* (Prabhu et al., 1965; Ramanamurthy et al., 1972; Padmakumar et al., 2010b). Therefore, it can be assumed that because of such bloom events, the shape diversity could be heavily influenced and skewed towards the bloom-forming dominant shape in the study area (NEAS-O and SEAS-O). Even considering such events, the eastern AS (NEAS-O and SEAS-O) is dominated by simple shape phytoplankton, particularly the Cyl-shape, suggesting it is the most adapted shape irrespective of the oceanographic regions and hydrographic conditions. The Cyl-shape has a wide morphological variability associated with wide taxonomic variability and is also considered as a more attenuated shape capable of conserving optimum S:V ratio very efficiently, therefore, making it the best fit with the prevailing environmental conditions (Aubry et al., 2017).

Variability in frontal and non-frontal regions

The mesoscale features (fronts or filaments), which are used to generate potential fisheries zone (PFZ) advisories, are considered hotspots for phytoplankton bloom (Franks, 1992; Hesse et al., 1989) and its formation both in coastal (Sarma et al., 2018; Vipin et al., 2015) and open ocean (Roy et al., 2015; Amol, 2018) regions of EAS is well documented. The phytoplankton community studies on frontal regions of the EAS are mostly based on marker pigments (Roy et al., 2015; Bernal et al., 2019; Kurian et al., 2020). However, detailed taxa and morphometry-based studies of the phytoplankton community variability in coastal and open ocean frontal regions are lacking and an attempt is made to delineate frontal influence on the phytoplankton shape dominance in EAS.

The phytoplankton shapes in EAS showed significant morphometric variability between NEAS-C and SEAS-O frontal regions. The frontal regions in NEAS-C were dominated by Cyl2Hs (43-56% and are solely represented by *Skeletonema*) and its dominance can be explained by the background condition or pre-existing phytoplankton community theory (Sarma et al., 2018). This suggests that Cyl2Hs-shaped phytoplankton was best adapted to exploit the frontal hydrographic

conditions. The morphometric adaptations like high S:V (0.8) associated with low GALD in Cyl2Hs might have a major role. The dominance of chain-forming diatoms in the coastal frontal regions is also reported in the South China Sea (Liu et al., 2021) and EAS (Sarma et al., 2018). However, the non-frontal (NF) regions were equally dominated by Cyl (*Leptocylindrus* being the dominant one), Cyl2Hs (23-22%, PoP (17%), and ElliP (15%) shapes. This suggests that the NF regions have a higher competition among the species for the limited resources where all the major shapes flourished similarly to their potential, whereas Cyl2Hs shape competes with others in frontal conditions. However, it should be noted that the phytoplankton response to the frontal conditions is subjected to the prevailing background conditions and community (Sarma et al., 2018; Kurian et al., 2020). The background phytoplankton community is dominated by chain-forming centric diatoms but the percentage contribution and abundance were relatively less. Also, the species composition (particularly diatoms) was slightly different in the non-front regions compared to the frontal regions. Such morphological shift towards a more attenuated shape (like long chain-forming *Skeletonema*) is a type of adaptation, which show minimal variations in the S:V ratio to maximize chloroplast exposition to light i.e. opting for the most elongated shape by maintaining the shortest diameter (Naselli-Flores & Barone., 2011).

In contrast to NEAS-C fronts, the shape dominance in the oligotrophic SEAS-O front is different despite both T1 and T2 transects showing the least shape diversity (only 12 shapes) with the former transect cutting across the frontal waters but not in the latter i.e. T2 transect without fronts (Bemal et al., 2019). SEAS is seldom enriched by Rossby wave-associated fronts bringing in changes in hydrographic conditions but is less favorable to phytoplankton growth compared to the NEAS (Supplementary Table 2). Nevertheless, this study points out the influence of Rossby fronts on phytoplankton shape dominance and biological productivity per se. The frontal stations in SEAS-O showed a slight increase in abundance and diversity compared to those of non-frontal stations located on the western side (NFW) but not those on the eastern side (NFE). The availability of relatively higher inorganic nitrogen in frontal (2.06 μ M) and NFE (1.54 μ M) than NFW (1.02 μ M) could be the reason for the differences in phytoplankton abundance. In NFE the increased abundance can also be due to the reminiscence of frontal signature (Vipin et al., 2015; Amol, 2018; Bemal et al., 2019) along the path as the sampled front was associated with a strong current that was drifting at 40-50 cm s⁻¹ westward (Bemal et al., 2019). The Rossby waves were drifting westward towards the offshore, which means that the NFE should have the reminiscence of the Rossby front, and NFW (yet to be influenced by the Rossby front) is the true non-frontal region which is also evident from the salinity profile of water mass as explained in Bemal et al., 2019 in details. The reminiscence effect of the

westward propagating Rossby front is also well reflected in the morphological and species diversity of the associated phytoplankton community. The dominance of the Cyl (41%) shape in the NFE and also the existence of the Elli-shape (7% though in less abundance) set the necessary background for the phytoplankton community, which took advantage of the Rossby front and co-dominated the frontal region. The frontal regions of SEAS-O were co-dominated by Elli (26%) and Cyl (21%) shapes representing dinoflagellate and centric diatoms, respectively. Even though dinoflagellates are considered poor competitors for inorganic nutrients (Litchman & Klausmeier, 2008), they are generally predominant in low-nutrient waters as observed in this study. For instance, the ability of *Gyrodinium* spp., Elli-shaped mixotrophic dinoflagellate, to rapidly increase almost three times and respond to the abrupt resource enrichment associated with the Rossby front proves that Elli-shaped phytoplankton has the required adaptive strategies (flagella and mixotrophy) to flourish in the given environmental conditions.

Conclusion

This study concludes that the phytoplankton cell shape in the eastern Arabian Sea showed a high level of redundancy by choosing only a few dominant shapes associated with high taxonomic diversity. The integrated approach (taxonomy and morphology) adopted in the present study revealed higher taxonomic and shape diversity in the convective mixing influenced non-oligotrophic NEAS-O than adjoining NEAS-C and oligotrophic SEAS-O. Interestingly the shape diversity and dominance (Cyl, ElliP, and PoP) remained the same between NEAS-O and SEAS-O, and among the fronts, the combined and simple shaped phytoplankton out-competed in NEAS-C and SEAS-O. The assessment of morphological properties based on S:V and its relationship with GALD suggested the prevalence of different adaptive strategies to cope with respective hydrographic conditions in the open ocean (NEAS-O and SEAS-O) and coastal (NEAS-C) by conserving S:V despite the increase in GALD in the former and no change in the later.

Acknowledgment

The authors are grateful to the Director of CSIR-National Institute of Oceanography for his support and encouragement. The authors also acknowledge the participants from the NIO-ship cell, the captain, and crew members of the cruises for helping us onboard. The support of Dr. V.V.S.S Sarma, Dr. D. V. Desai, and Dr. M. S. Krishna is gratefully acknowledged. We thank the two anonymous reviewers for their valuable suggestions for improving the manuscript. The first author also acknowledges UGC

for fellowship. This is an NIO contribution no.....

Author contributions

Pranoy Paul: Sample collection, samples analysis, data analysis, and interpretation, manuscript writing

Jagadish S. Patil: Original concept, sample collection, data interpretation, and manuscript elaboration;

AC Anil: Manuscript elaboration and also co-supervised all works.

Funding information

This work is supported by the CSIR-National Institute of Oceanography Ocean Finder project (PSC0105).

Availability of data and materials

All data concerning the study are included in this manuscript and some are also provided as supplementary. However, it does not apply to material availability.

Ethics declaration

“All authors have read, understood, and have complied as applicable with the statement on "Ethical responsibilities of Authors" as found in the Instructions for Authors and are aware that with minor exceptions, no changes can be made to authorship once the paper is submitted.”

Competing interest

The authors declare that they have no known competing financial interests or personal relationships that could have appeared to influence the work reported in this paper.

References

Alexander, H., Rouco, M., Haley, S.T., Wilson, S.T., Karl, D.M., & Dyhrman, S.T. (2015) Functional group-specific traits drive phytoplankton dynamics in the oligotrophic ocean. *Proceedings of the National Academy of Sciences*, 112(44), E5972-E5979.

Amol, P. (2018) Impact of Rossby waves on chlorophyll variability in the southeastern Arabian Sea. *Remote Sensing Letters*, Vol. 9, No. 12, 1214–1223.

Aubry, B.F., Pugnetti, A., Roselli, L., Stanca, E., Acri, F., Finotto, S., & Basset, A. (2017) Phytoplankton morphological traits in a nutrient-enriched, turbulent Mediterranean microtidal lagoon. *Journal of Plankton Research*, 39(3), 564-576.

Ault, T., Velzeboer, R. & Zammit, R. (2000) Influence of nutrient availability on phytoplankton growth and community structure in the Port Adelaide River, Australia: bioassay assessment of potential nutrient limitation. *Hydrobiologia*, 429: 89-103.

- Banase K. (1987) Seasonality of phytoplankton chlorophyll in the central and northern Arabian Sea. *Deep-Sea Research*, Vol. 34, (5-6), 713-723.
- Barton, A.D., Pershing, A.J., Litchman, E., Record, N.R., Edwards, K.F., Finkel, Z.V., Kiørboe, T. & Ward, B.A. (2013) The biogeography of marine plankton traits. *Ecology Letters*, 16(4), 522-534.
- Bemal, S., Anil, A.C. & Amol, P. (2019) Picophytoplankton variability: Influence of Rossby wave propagation in the southeastern Arabian Sea. *Journal of Marine Systems*, 199, 103-221.
- Bemal, S., Anil, A.C., Shankar, D., Remya, R & Roy, R. (2018) Picophytoplankton variability: Influence of winter convective mixing and advection in the northeastern Arabian Sea. *Journal of Marine Systems*, 180, 37–48.
- Breton, E., Christaki, U., Bonato, S., Didry, M., & Artigas, L. F. (2017) Functional trait variation and nitrogen use efficiency in temperate coastal phytoplankton. *Marine Ecology Progress Series*, 563, 35-49.
- Capblancq, J. & Catalan, J. (1994) Phytoplankton: which, and how much? In Margalef, R. (ed.), *Limnology Now: A Paradigm of Planetary Problems*. Elsevier Science B.V, Amsterdam, pp. 9–36.
- Chandrasekhararao, A.V., Kurian, S., Vidya, P.J., Gauns, M., Shenoy, D.M., Mulla, A., Naik, H., Reddy, T.V & Naqvi, S.W.A. (2018) Phytoplankton response to the contrasting physical regimes in the eastern Arabian Sea during northeast monsoon. *Journal of Marine Systems*, 182, 56–66.
- Chisholm, S. W. (1992). Phytoplankton size. *Primary productivity and biogeochemical cycles in the sea*, Plenum Press, New York, G.P. Falkowski, A.D. Woodhead (Eds.) 213-237.
- Chitari, R. R. & Anil, A.C. (2017) Estimation of diatom and dinoflagellate cell volumes from surface water of the Northern Indian Ocean. *Oceanologia*, 59, 389-395.
- D'Silva, M.S., Anil, A.C., Naik, R.K & D'Costa, P.M. (2012) Algal blooms: a perspective from the coasts of India. *Natural Hazards*, 63, 1225–1253.
- Duarte, C.M., Agusti, S., & Canfield Jr, D.E. (1990) Size plasticity of freshwater phytoplankton: implications for community structure. *Limnology and Oceanography*, 35(8), 1846-1851.
- Durante, G., Basset, A., Stanca, E. & Roselli, L. (2019) Allometric scaling and morphological variation in sinking rate of phytoplankton. *Journal of Phycology*, 55, 1386–1393.
- Finkel, Z.V., Beardall, J., Flynn, K.J., Quigg, A., Rees, T.A.V., & Raven, J.A. (2010). Phytoplankton in a changing world: cell size and elemental stoichiometry. *Journal of plankton research*, 32(1), 119-137.
- Finkel, Z.V. (2007) Does phytoplankton cell size matter? The evolution of modern marine food webs. *Evolution of primary producers in the Sea*, 1:333-350.
- Fraisse, S., Bormans, M., & Lagadeuc, Y. (2013) Morphofunctional traits reflect differences in phytoplankton community between rivers of contrasting flow regime. *Aquatic Ecology*, 47(3), 315-327.
- Franks, P.J. (1992) Phytoplankton blooms at fronts: patterns, scales, and physical forcing mechanisms. *Reviews in Aquatic Sciences*, 6, 121–137.

- Gomes, H.R., Goes, J.I., Matondkar, S.G.P., Parab, S.G., Al-Azri, A.R.N. & Thoppil, P.G. (2008) Blooms of *Noctiluca miliaris* in the Arabian Sea—An in situ and satellite study. *Deep-Sea Research-I*, 55, 751–765.
- Grover, J.P. (1989) Influence of cell shape and size on algal competitive ability. *Journal of Phycology*, 25, 402–405.
- Hesse, K.J., Liu, Z.L. & Schaumann, K. (1989) Phytoplankton and fronts in the German Bight. *Scientia Marina*, 53, 187–196.
- Hillebrand, H., Durselen, C.D., Kirschtel, D., Pollinger, U. & Zohary, T. (1999) Biovolume calculation for pelagic and benthic microalgae. *Journal of Phycology*, 35, 403–424.
- Kruk, C., Huszar, V.L., Peeters, E.T., Bonilla, S., Costa, L., Lüring, M., Reynolds, C.S. & Scheffer, M. (2010) A morphological classification capturing functional variation in phytoplankton. *Freshwater biology*, 55(3), 614–627.
- Kumar, P.S., Narvekar, J., Kumar, A., Shaji, C., Anand, P., Sabu, P., Rijomon, G., Josia, J., Jayaraj, K. & Radhika, A. (2004) Intrusion of the Bay of Bengal water into the Arabian Sea during winter monsoon and associated chemical and biological response. *Geophysical Research Letters*, 31, 15.
- Kurian, S., Chndrasekhararao, A.V., Vidya, P.J., Shenoy, D.M., Gauns, M., Uskaikar, H. & Aparna, S.G. (2020) Role of oceanic fronts in enhancing phytoplankton biomass in the eastern Arabian Sea during an oligotrophic period. *Marine Environmental Research*, 160, 105023.
- Lauria, M.L., Purdie, D.A. & Sharples, J. (1999) Contrasting phytoplankton distribution controlled by tidal turbulence in an estuary. *Journal of Marine Systems*, 21, 189–197.
- Lavorel, S. and Garnier, E. (2002) Predicting changes in community composition and ecosystem functioning from plant traits: Revisiting the Holy Grail. *Functional Ecology*, 16, 545–556.
- Levine, J. M. (2016) A trail map for trait-based studies. *Nature*, 529, 163–164.
- Lewis, W.M. (1976) Surface/volume ratio: Implication for phytoplankton morphology. *Science*, 192, 885–887.
- Litchman, E. & Klausmeier, C. A. (2008) Trait-based community ecology of phytoplankton. *The Annual Review of Ecology, Evolution, and Systematics*, 39, 615–639.
- Litchman, E., Klausmeier, C. A., Schofield, O. M., & Falkowski, P. G. (2007) The role of functional traits and trade-offs in structuring phytoplankton communities: scaling from cellular to ecosystem level. *Ecology Letters*, 10(12), 1170–1181.
- Liu, Z., Li, Q.P., Ge, Z & Shuai, Y. (2021) Variability of plankton size distribution and controlling factors across a coastal frontal zone. *Progress in Oceanography*, 197, 102665.
- Madhupratap, M., Kumar, S.P., Bhattathiri, P.M.A., Kumar, M.D., Raghukumar, S., Nair, K.K. C., & Ramaiah, N. (1996) Mechanism of the biological response to winter cooling in the northeastern Arabian Sea. *Nature*, 384(6609), 549–552.
- Margalef, R. (1978) Life-forms of phytoplankton as survival alternatives in an unstable environment. *Oceanologica Acta*, 493–509.

- Martini, S., Larras, F., Boyé, A., Faure, E., Aberle, N., Archambault, P., Bacouillard, L., Beisner, B.E., Bittner, L., Castella, E. & Danger, M., (2021) Functional trait-based approaches as a common framework for aquatic ecologists. *Limnology and Oceanography*, 66(3), 965-994.
- McGill, B.J., Enquist, B.J., Weiher, E. & Westoby, M. (2006) Rebuilding community ecology from functional traits. *Trends in Ecology & Evolution*, 21, 178–185.
- Naselli-Flores L, Padisak J & Albay M. (2007) Shape and size in phytoplankton ecology: Do they matter? *Hydrobiologia*, 578, 157–161.
- Naselli-Flores, L & Barone, R. (2011) Fight on plankton! or, phytoplankton shape and size as adaptive tools to get ahead in the struggle for life. *Cryptogamie, Algologie*, 32(2):157-204.
- Naselli-Flores, L. (2014) Morphological analysis of phytoplankton as a tool to assess ecological state of aquatic ecosystems: the case of Lake Arancio, Sicily, Italy. *Inland Waters*, 4(1), 15-26.
- Naselli-Flores, L. & Barone, R. (2007) Pluriannual morphological variability of phytoplankton in a highly productive Mediterranean reservoir (Lake Arancio, Southwestern Sicily). *Hydrobiologia*, 578, 87–95.
- Padisak, J., Soroczki-Pinter, E & Reznér, Z. (2003) Sinking properties of some phytoplankton shapes and the relation of form resistance to morphological diversity of plankton – an experimental study. *Hydrobiologia*, 500, 243–257.
- Padmakumar, K.B., Menon, N.R. & Sanjeevan, V.N. (2010) Occurrence of endosymbiont *Richelia intracellularis* (Cyanophyta) within the diatom *Rhizosolenia hebetata* in Northern Arabian Sea. *International Journal of Biodiversity and Conservation*, 2(4), 70-74.
- Padmakumar, K.B., Smitha, B.R., Thomas, L.C., Fanimol, C.L., SreeRanjimma, G., Menon, N.R. & Sanjeevan, V.N. (2010b) Blooms of *Trichodesmium erythraeum* in the South Eastern Arabian Sea during the onset of 2009 Summer Monsoon. *Ocean Science Journal*, 45 (3), 151–157.
- Paul, P., Patil, J.S. & Anil, A.C. (2021) Phytoplankton communities in marine intertidal rock-pools: Effect of location, geometric shapes and allelopathy. *Journal of Earth System Science*, 130 (3), 1-17.
- Prabhu M.S., Ramamurthy S., Kuthalingam M.D.K & Dhulkhed M.H. (1965) On an unusual swarming of the planktonic blue-green algae *Trichodesmium* spp., off Mangalore. *Current Science*, 34(3), 95-95.
- R core Team (2020) R: A language and environment for statistical computing. R foundation for statistical computing, Vienna, Austria. <https://www.R-project.org/>.
- Ramanamurthy V.D., Selvakumar R.A. & Bhargava R.M.S. (1972) Studies on the blooms of *Trichodesmium erythraeum* (Ehr.) in the waters of the central west coast of India. *Current Science*, 41, 803–804.
- Reynolds, C. S. (1997) *Vegetation processes in the pelagic: a model for ecosystem theory*. Ecology Institute, Oldendorf Luhe, Germany, 371.
- Roselli, L., & Basset, A. (2015) Decoding size distribution patterns in marine and transitional water phytoplankton: from community to species level. *PloS one*, 10(5), e0127193.

- Roy, R., Chitari, R., Kulkarni, V., Krishna, M.S., Sarma, V.V.S.S., & Anil, A.C. (2015) CHEMTAX-derived phytoplankton community structure associated with temperature fronts in the northeastern Arabian Sea. *Journal of Marine Systems*, 144, 81-91.
- Ryabov, A., Kerimoglu, O., Litchman, E., Olenina, I., Roselli, L., Basset, A., Stanca, E. & Blasius, B. (2021) Shape matters: the relationship between cell geometry and diversity in phytoplankton. *Ecology Letters*, 24(4), pp.847-861.
- Salmaso, N. & Padisak, J. (2007) Morpho-functional groups and phytoplankton development in two deep lakes (Lake Garda, Italy and Lake Stechlin, Germany). *Hydrobiologia*, 578, 97–112.
- Sarma, V.V.S.S., Desai, D.V., Patil, J.S., Khandeparker, L., Aparna, S.G., Shankar, D., D'Souza, S., Dalabehera, H.B., Mukherjee, J., Sudharani, P. & Anil, A.C. (2018) Ecosystem response in temperature fronts in the northeastern Arabian Sea. *Progress in Oceanography*, 165, 317–331.
- Sarma, V.V.S.S., Patil, J.S., Shankar, D. & Anil, A.C. (2019) Shallow convective mixing promotes massive *Noctiluca scintillans* bloom in the northeastern Arabian Sea. *Marine Pollution Bulletin*, 138, 428-436.
- Sawant S & Madhupratap M. (1996) Seasonality and composition of phytoplankton in the Arabian Sea. *Current Science*, 71, 11.
- Schlitzer, R. (2015) Ocean Data View, <http://odv.awi.de>.
- Segura, A. M., Kruk, C., Calliari, D., & Fort, H. (2013) Use of a morphology-based functional approach to model phytoplankton community succession in a shallow subtropical lake. *Freshwater Biology*, 58(3), 504-512.
- Shankar, D., Vinayachandran, P. & Unnikrishnan, A. (2002) The monsoon currents in the north Indian Ocean. *Progress in Oceanography*, 52, 63–120.
- Shenoi, S., Shankar, D. & Shetye, S. (2002) Differences in heat budgets of the near-surface Arabian Sea and Bay of Bengal: implications for the summer monsoon. *Journal of Geophysical Research: Oceans*, 107, 1–14.
- Simberloff, D. & Dayan, T. (1991) The guild concept and the structure of ecological communities. *Annual Review of Ecology and Systematics*, 22, 115–143.
- Smayda, T.J. (1970) The suspension and sinking of phytoplankton in the sea. *Oceanography Marine Biology Annual Revision*, 8, 353-414.
- Smayda, T.J., & Boleyn, B.J. (1966) Experimental observations on the flotation of marine diatoms. II. *Skeletonema costatum* and *Rhizosolenia setigera*. *Limnology and Oceanography*, 11(1), 18-34.
- Stanca, E., Cellamare, M., & Basset, A. (2013) Geometric shape as a trait to study phytoplankton distributions in aquatic ecosystems. *Hydrobiologia*, 701(1), 99-116.
- Sun, J., & Liu, D. (2003) Geometric models for calculating cell biovolume and surface area for phytoplankton. *Journal of Plankton Research*, 25(11), 1331-1346.

- Taylor, F. J. R. (1973). General features of dinoflagellate material collected by the “Anton Bruun” during the International Indian Ocean Expedition. In *The biology of the Indian Ocean*. Springer, Berlin, Heidelberg, 155-169.
- Thingstad, T.F., Krom, M.D., Mantoura, R.F.C., Flaten, G.F., Groom, S., Herut, B., Kress, N., Law, C.S., Pasternak, A., Pitta, P. & Psarra, S. (2005) Nature of phosphorus limitation in the ultraoligotrophic eastern Mediterranean. *Science*, 309(5737), 1068-1071.
- Tomas, C. R. (Ed.). (1997). Identifying marine phytoplankton. Academic Press, San Diego, Elsevier.
- Vijayan, A.K., Reddy, B.B., Sudheesh, V., Marathe, P.H., Nampoothiri, V.N., Harikrishnachari, N.V., Kavya, P., Gupta, G.V.M. & Ramanamurthy, M.V. (2021) Phytoplankton community structure in a contrasting physico-chemical regime along the eastern Arabian Sea during the winter monsoon. *Journal of Marine Systems*, 215, 103501.
- Vipin, P., Sarkar, K., Aparna, S.G., Shankar, D., Sarma, V.V.S.S., Gracias, D.G., Krishna, M.S., Srikanth, G., Mandal, R., Rama Rao, E.P. & Rao, S.N. (2015) Evolution and subsurface characteristics of a sea-surface temperature filament and front in the northeastern Arabian Sea during November–December 2012. *Journal of Marine Systems*, 150, 1–11.
- Weithoff, G. & Gaedke, U. (2017) Mean functional traits of lake phytoplankton reflect seasonal and inter-annual changes in nutrients, climate and herbivory. *Journal of Plankton Research*, 39, 509–517.
- Weithoff, G. & Beisner, B.E. (2019) Measures and approaches in trait-based phytoplankton community ecology—from freshwater to marine ecosystems. *Frontiers in Marine Science*, 6, 40.
- Wiggert, J. D., Hood, R. R., Banse, K., & Kindle, J. C. (2005) Monsoon-driven biogeochemical processes in the Arabian Sea. *Progress in Oceanography*, 65(2-4), 176-213. Williams, O. J., Beckett, R. E., & Maxwell, D. L. (2016) Marine phytoplankton preservation with Lugol’s: a comparison of solutions. *Journal of Applied Phycology*, 28(3), 1705-1712.

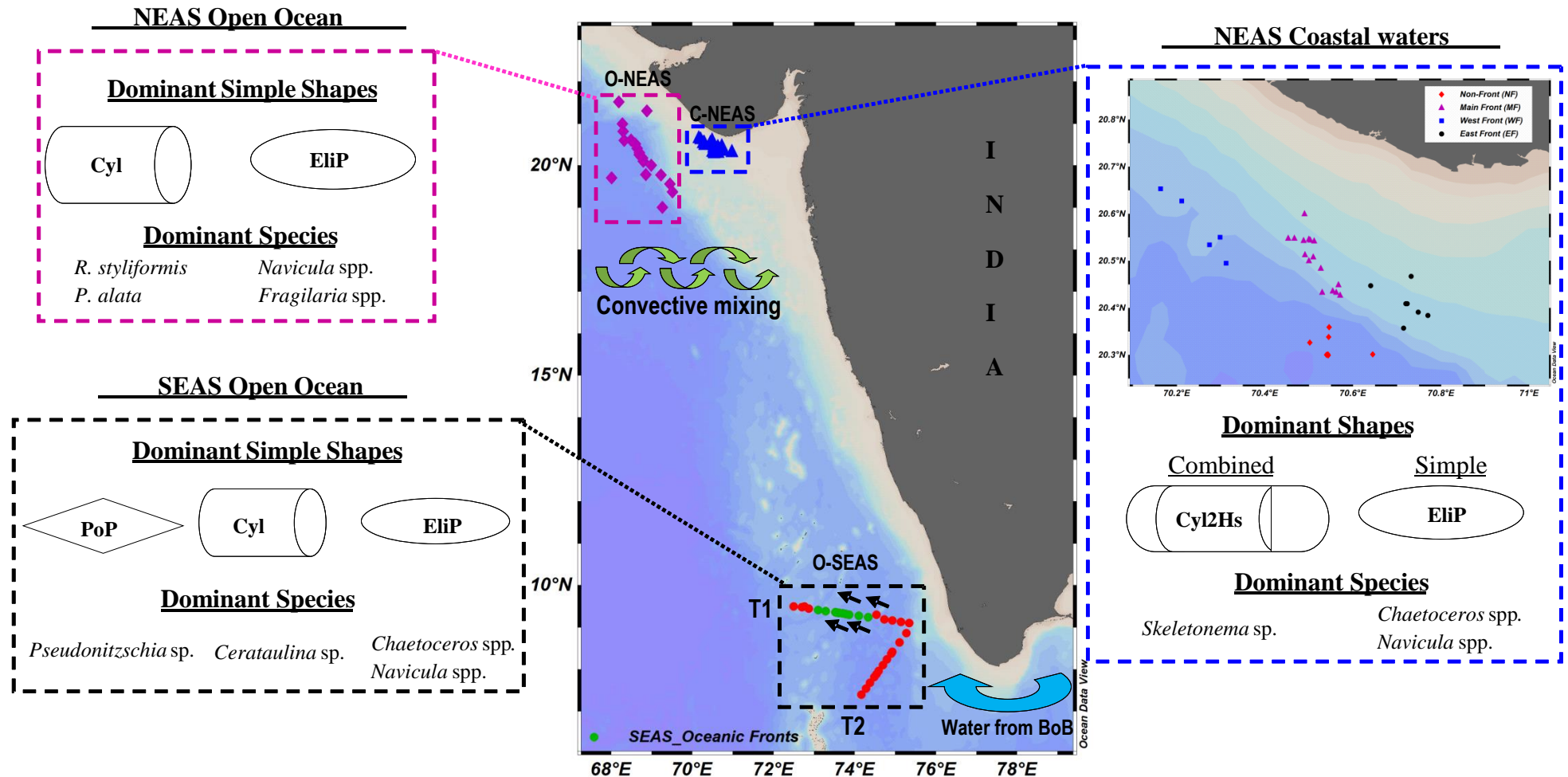


Fig. 1. Schematic showing location of the stations in the NEAS (both ocean and coastal) and SEAS (only ocean) along with the dominant taxa and shape and the prevailing hydrographic conditions. Green, blue and black arrow indicates convective mixing, inflow of water from BOB and Rossby wave. Note: Cyl: cylinder, Ellip: elliptic prism, POP: Prism on parallelogram, Cyl2Hs: cylinder+2 half sphere. T1 and T2 corresponds to transect 1 and 2 in SEAS-O

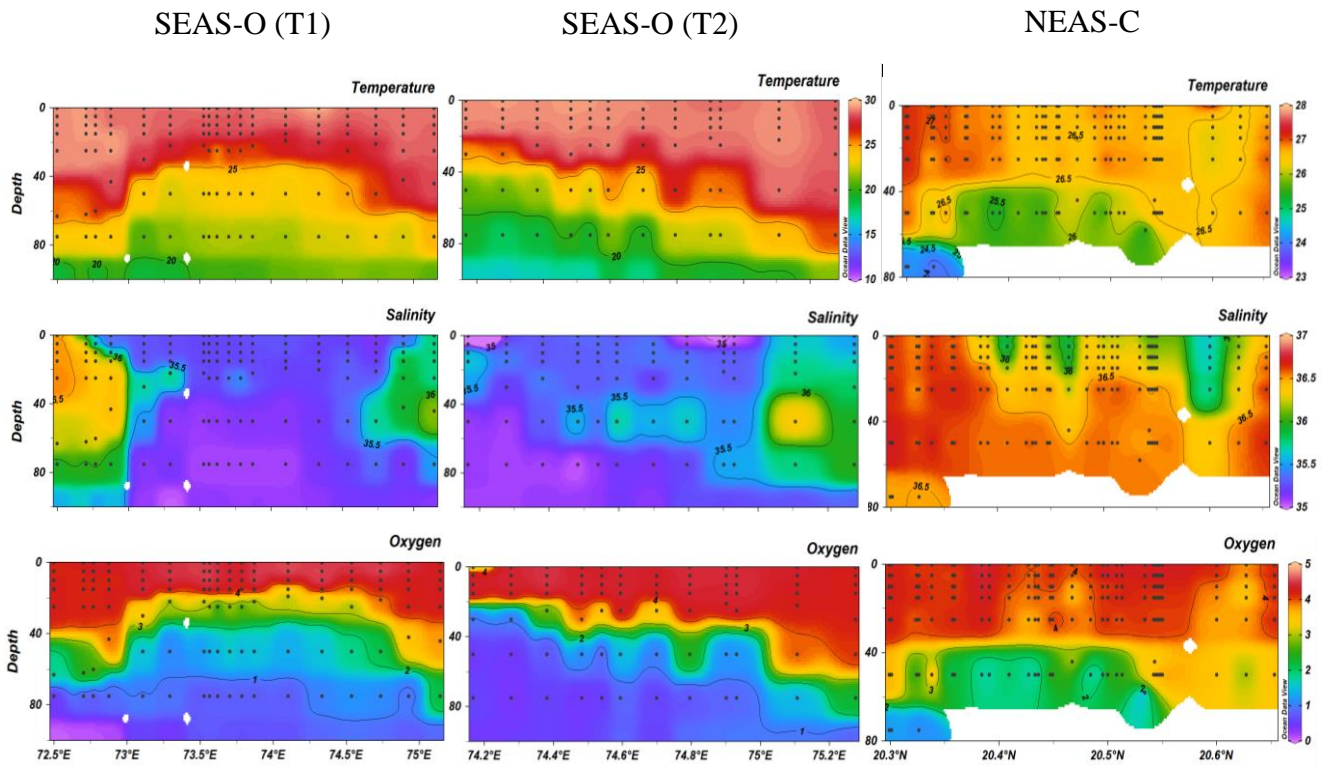


Fig. 2. The vertical distribution of temperature ($^{\circ}\text{C}$), salinity (psu) and oxygen concentration (mL L^{-1}) in NEAS-C and SEAS-O.

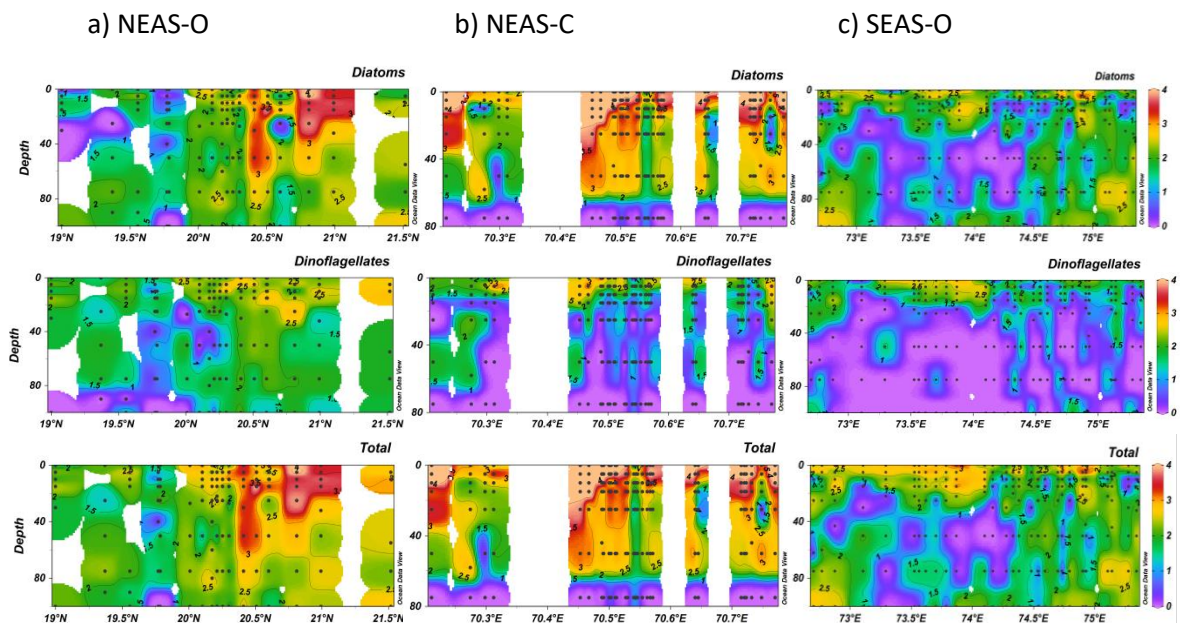


Fig. 3. Groupwise distribution of phytoplankton in the water column of NEAS and SEAS. NEAS-O: North-eastern Arabian Sea open ocean; NEAS-C: North-eastern Arabian Sea coastal region and SEAS-O: South-eastern Arabian Sea open ocean.

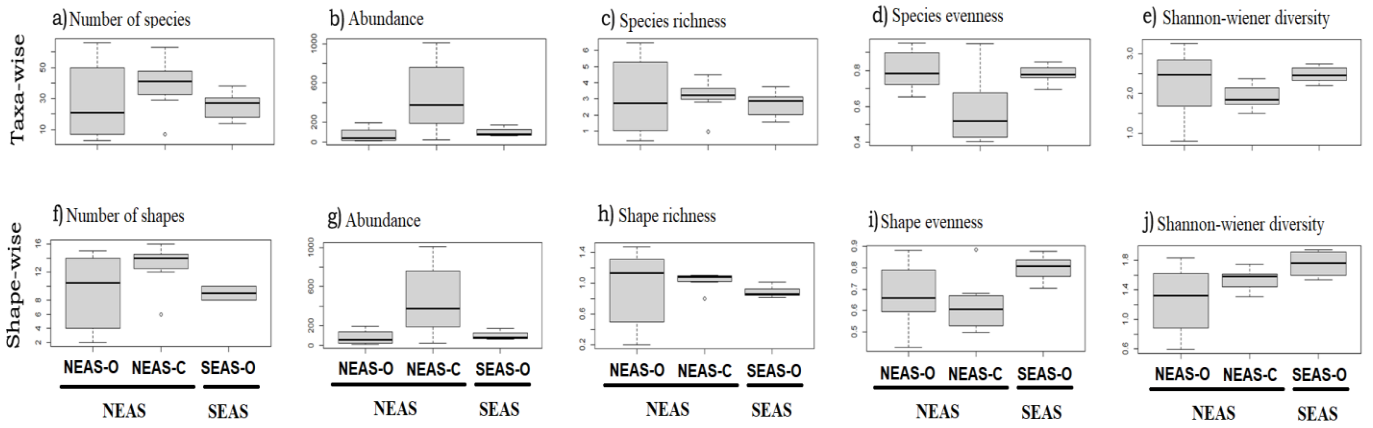


Fig. 4. Univariate measures of phytoplankton (both taxonomy and shape-wise) from NEAS (both coastal and open ocean) and SEAS (open ocean). Station data are pooled and presented here.

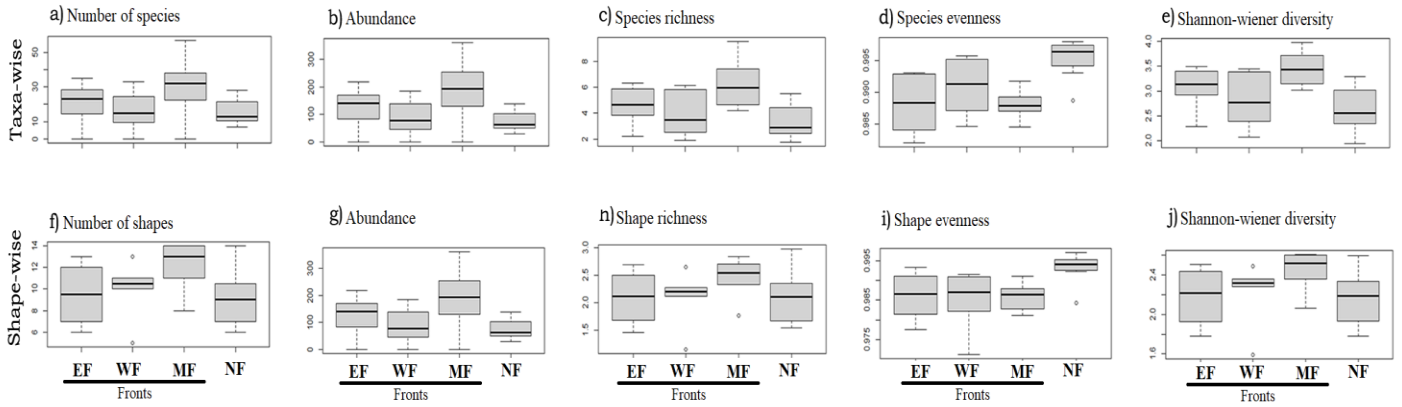


Fig. 5. Univariate measures of phytoplankton (both taxonomy and shape-wise) from frontal and non-frontal in coastal region of NEAS. EF: East front; WF: West front; MF: Main front and NF: Non-front. Station data frontal and non-frontal region are pooled and presented here.

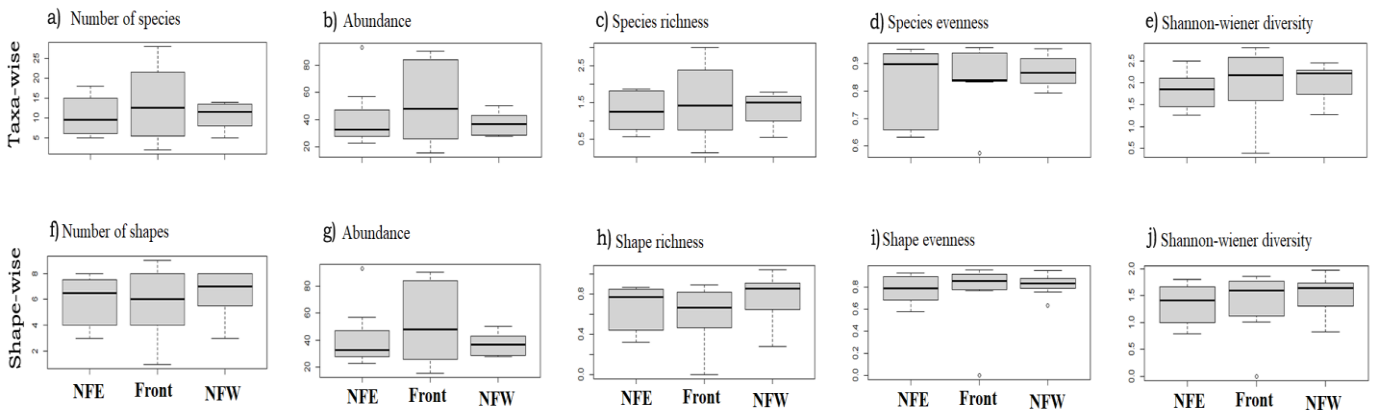


Fig. 6. Univariate measures of phytoplankton (both taxonomy and shape-wise) from frontal and non-frontal in oceanic region of SEAS. NFW: Non-front West; F: Frontal region and NFE: Non-front East. Station data frontal and non-frontal region are pooled and presented here.

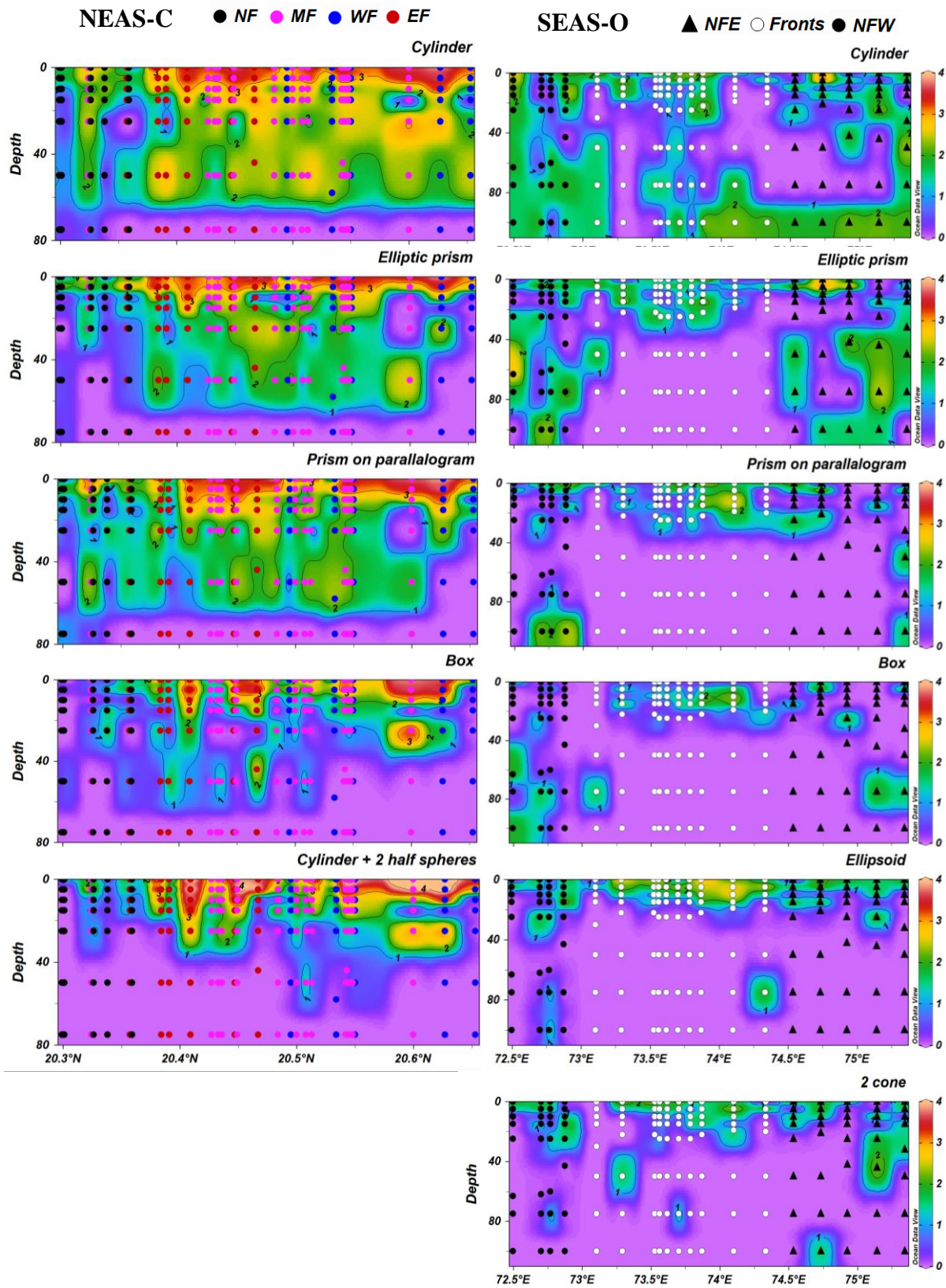


Fig. 7. Distribution of dominant phytoplankton shape in the frontal and non-frontal water column of NEAS and SEAS. NEAS-C: Coastal North-eastern Arabian Sea; SEAS-O: Open Ocean South-eastern Arabian Sea; NF: Non-front; MF: Main front; WF: West front; EF: East front; NFE: Non-front East and NFW: Non-front West.

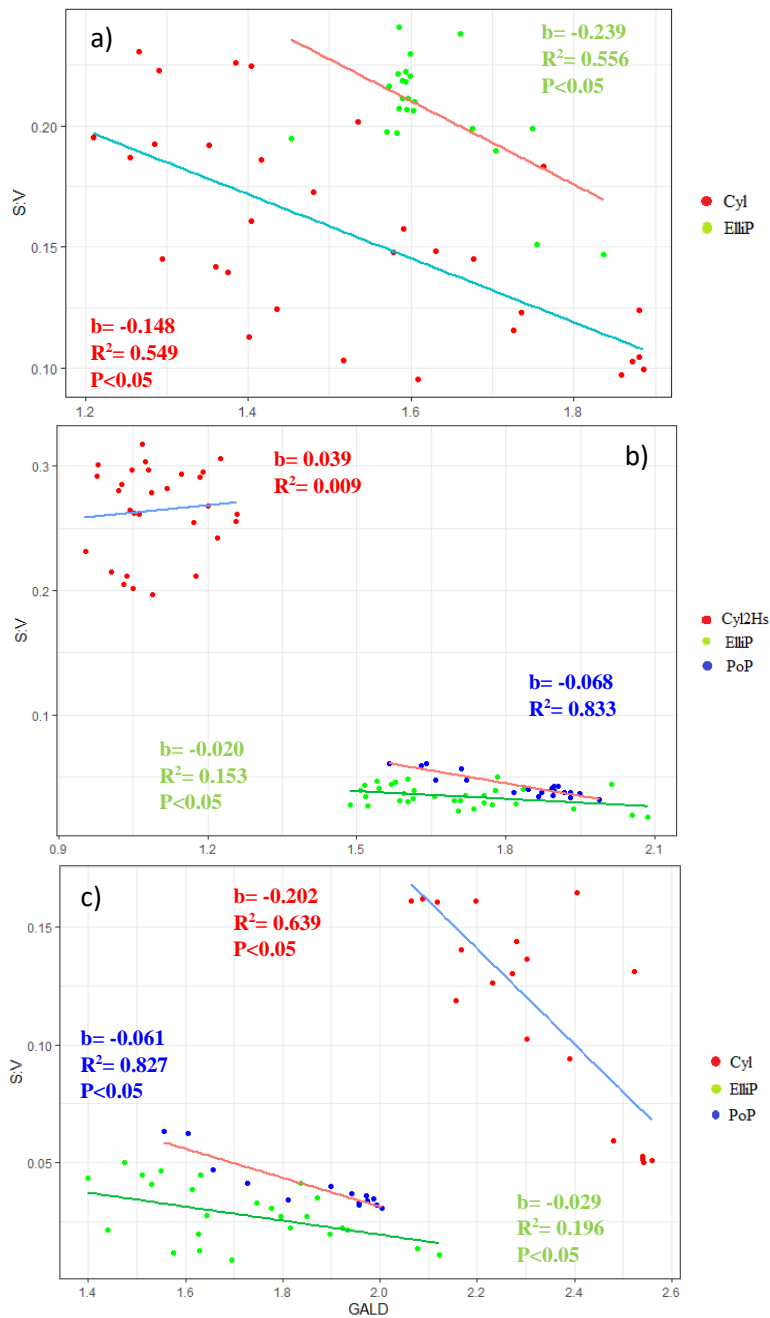


Fig. 8. Relationship between GALD and S:V for the 8 dominant shapes recorded in North-eastern (NEAS-O and NEAS-C) and South-eastern Arabian Sea during the study period. a) NEAS-O: North-eastern Arabian Sea open-ocean, b) NEAS-C: North-eastern Arabian Sea coastal waters, and c) SEAS-O: South-eastern Arabian Sea open ocean; Cyl: Cylinder; EliP: Elliptic prism; Cyl2Hs: Cylinder + 2 Half sphere; PoP: Prism on parallelogram.

Supplementary Table 1. Hydrography and nutrient concentration at surface and sub-surface in NEAS-O, NEAS-C and SEAS-O in winter monsoon. Mean value is calculated for temperature, salinity and oxygen concentration. The median value is used for nutrient concentration. The numbers in parenthesis indicate range values of the parameter and the * indicates the value of chlorophyll concentration.

Regions of EAS	Cruise	Temperature (°C)	Salinity (psu)	Oxygen (mL L ⁻¹)	Fluorescence (mg/m ³)	Nitrate (µM)	Phosphate (µM)
NEAS-O	(0m)	26.1 (25.1–27.0)	36.3 (35.8–36.5)	4.3 (4.0–4.5)	0.54 (µg L ⁻¹)*	0.95 (0.56–3.23)	0.27 (0.09–0.45)
	(100m)	23.7 (19.5–25.0)	36.5 (36.2–36.7)	3.0 (0.3–4.1)	-	5.80 (3.17–17.0)	0.82 (0.41–1.77)
NEAS-C	(0m)	26.8 (26.3–27.3)	36.3 (35.5–36.7)	4.2 (3.7–4.6)	1.1 (0.2–3.0)	-	-
	(100m)	25.9 (24.0–27.1)	36.6 (36.3–36.7)	2.5 (0.9–4.1)	0.3 (0.2–0.5)	-	-
SEAS-O	T1 (0m)	28.9 (28.5–29.7)	35.4 (35.1–36.5)	4.4 (4.2–4.6)	0.6 (0.1–1.7)	0.96 (0.15–1.67)	0.24 (0.06–0.69)
	T1 (100m)	20.3 (18.8–21.6)	35.2 (35.0–35.7)	0.61 (0.07–0.93)	0.06 (0.003–0.2)	15.1 (10–20.9)	1.2 (1.0–1.9)
	T2 (0m)	29.1 (28.6–29.4)	33.8 (18.6–35.7)	4.3 (3.1–4.5)	0.62 (0.14–1.04)	-	-
	T2 (100m)	18.3 (16.5–21.5)	35.2 (35.1–35.3)	0.7 (0.5–1.0)	0.11 (0.002–0.24)	-	-

Supplementary Table 2. Hydrography and nutrient concentration at surface and sub-surface frontal and non-frontal regions of NEAS-C and SEAS-O in winter monsoon. The mean value is calculated for temperature, salinity, and oxygen concentration. The median value is used for nutrient concentration. The numbers in parentheses indicate the range values of the parameter.

Regions of EAS	Cruise	Temperature (°C)	Salinity (psu)	Oxygen (mL L⁻¹)	Fluorescence (mg/m³)	
NEAS-C	East Front (0m)	26.6 (26.4-27.1)	36 (35.6-36.6)	4.2 (3.9-4.6)	1.7 (1.1-3)	
	East Front (100m)	25.7 (24.8-26.4)	36.5 (36.4-36.6)	2.2 (1.6-3.1)	0.2 (0.2-0.3)	
	West Front (0m)	26.8 (26.3-27.1)	36.5 (36.1-36.7)	4.1 (3.7-4.2)	0.6 (0.4-0.9)	
	West Front (100m)	26.1 (24.9-27)	36.6 (36.5-36.7)	2.5 (0.5-4.1)	0.4 (0.2-0.5)	
	Main Front (0m)	26.7 (26.4-27.1)	36.2 (35.5-36.6)	4.2 (3.8-4.6)	1.4 (0.8-2.2)	
	Main Front (100m)	26.1 (25.4-26.8)	36.5 (36.3-36.6)	2.7 (1.6-3.9)	0.3 (0.2-0.4)	
	Non-Front (0m)	27.1 (27-27.3)	36.7 (36.6-36.7)	4.2 (4.1-4.2)	1.4 (0.2-9.4)	
	Non-Front (100m)	25.7 (24-27.1)	36.6 (36.5-36.7)	2.4 (1.1-4.1)	0.3 (0.2-0.5)	
	SEAS-O	Non-front West (0m)	29.1 (28.8-29.5)	35.8 (35.3-36.5)	4.3 (4.2-4.4)	0.3 (0.1-0.7)
		Non-front West (100m)	19.6 (18.8-20.6)	35.6 (35.5-35.7)	0.11 (0.07-0.14)	0.18 (0.15-0.20)
Front (0m)		28.9 (28.5-29.7)	35.3 (35.2-35.3)	4.5 (4.3-4.6)	0.8 (0.3-1.7)	
Front (100m)		20.3 (19-21.2)	35.1 (35-35.1)	0.7 (0.5-0.9)	0.02 (0.003-0.06)	
Non-front East (0m)		28.9 (28.7-29.2)	35.4 (35.1-35.8)	4.4 (4.3-4.5)	0.5 (0.1-0.8)	
Non-front East (100m)		21.1 (20.7-21.6)	35.2 (35.1-35.2)	0.8 (0.7-0.9)	0.1 (0.06-0.1)	

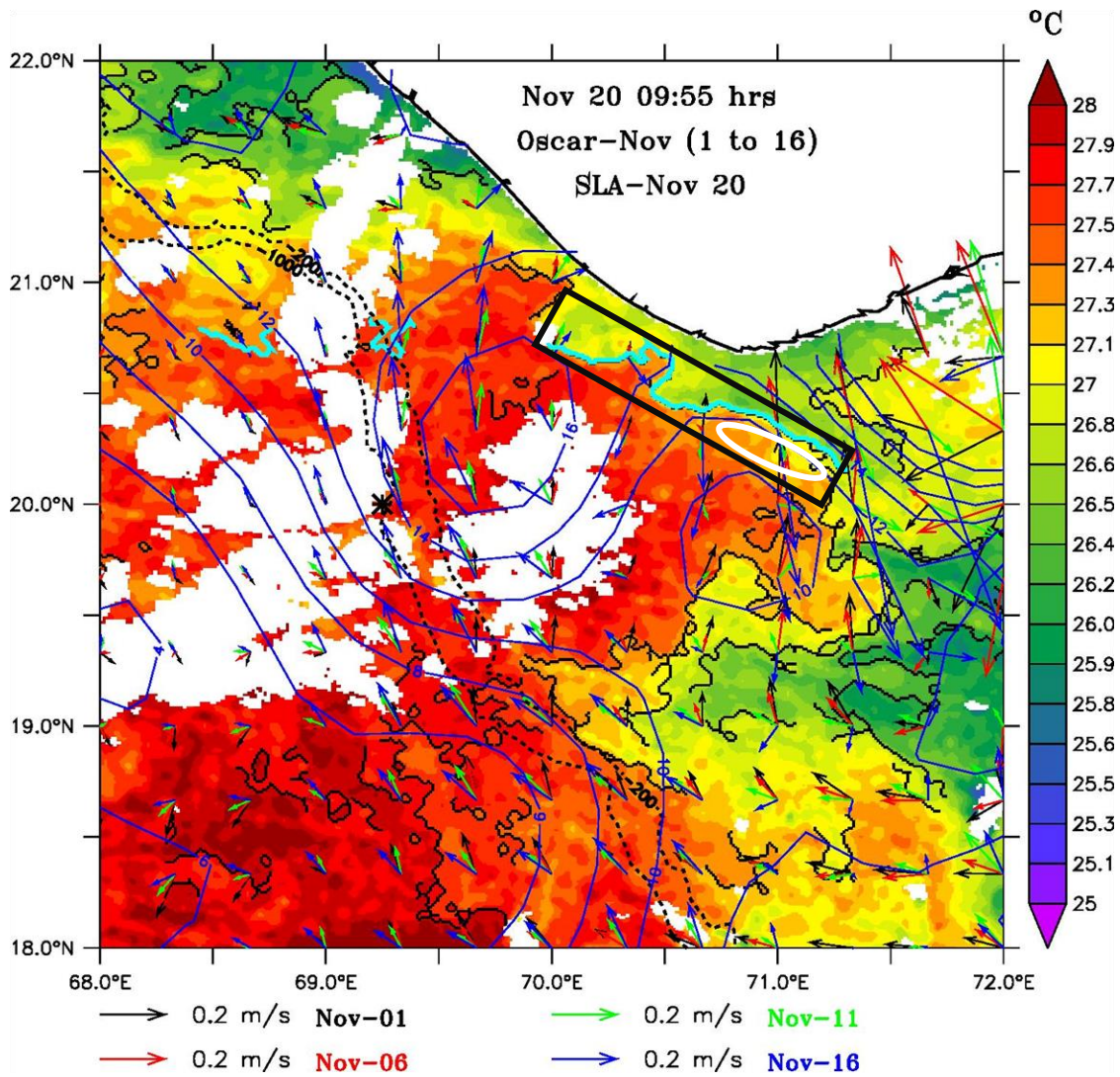
Supplementary Table 3. Micro-phytoplankton abundance (depth-averaged *cells L⁻¹*) and the corresponding shape in the open ocean and coastal region of North-eastern Arabian Sea (NEAS-O and NEAS-C) and open ocean of South-eastern Arabian Sea (SEAS-O). Species in bold font indicate diatoms and normal font indicates dinoflagellates; numbers in parenthesis are numbers of shapes recorded.

SI No.	Species	NEAS-O	NEAS-C	SEAS-O	Shapes
1.	<i>G. polygrammum</i>	0	0	4	
2.	<i>Gonyaulax kofoidii</i>	0	2	2	
3.	<i>Gonyaulax sp</i>	38	14	24	
4.	<i>Protoperidinium diabolus</i>	9	0	0	2 Cones (1)
5.	<i>Protoperidinium pallidum</i>	0	0	22	
6.	<i>Protoperidinium sp1</i>	378	398	203	
7.	<i>Protoperidinium sp2</i>	109	0	0	
8.	<i>Protoperidinium tenuissimum</i>	0	0	44	
9.	<i>Lioloma sp</i>	1312	0	0	
10.	<i>Synedra sp</i>	4	0	34	
11.	<i>Tabellaria sp.</i>	0	468	0	
12.	<i>Thalassionema nitzschioides</i>	6	4562	24	Box (2)
13.	<i>Thalassiothrix longissima</i>	60	0	0	
14.	<i>Thalassiothrix sp</i>	107	65	875	
15.	<i>Pinnularia</i>	0	134	0	
16.	<i>Asterionella sp.</i>	1	39	0	Box + 2 Cylinder (3)
17.	<i>Climacosphenia sp</i>	38	0	0	Box + Elliptic prism (4)
18.	<i>Podolampus palmipes</i>	2	12	0	
19.	<i>Podolampus sp</i>	12	16	0	
20.	<i>Podolampus spinifera</i>	3	0	0	Cone (5)
21.	<i>Pronoctiluca sp</i>	1	0	0	Cone + Half sphere (6)
22.	<i>Amphisolenia asrragalus</i>	5	0	0	
23.	<i>Amphisolenia asymmetric</i>	2	0	0	
24.	<i>Amphisolenia bidentata</i>	0	1	0	
25.	<i>Amphisolenia globifera</i>	3	0	0	
26.	<i>Amphisolenia sp</i>	5	0	0	
27.	<i>Asteriomphalus sp</i>	7	27	20	
28.	<i>Bacteriastrum sp</i>	1	0	0	
29.	<i>Ceratulina sp</i>	207	216	502	Cylinder (7)
30.	<i>Coscinodiscus sp</i>	326	105	85	
31.	<i>Cyclotella sp</i>	22	0	0	
32.	<i>Dactylosolen sp</i>	0	26	0	
33.	<i>Guinardia flaccida</i>	0	0	2	
34.	<i>Guinardia sp</i>	36	60	0	
35.	<i>Guinardia striata</i>	190	4	2	

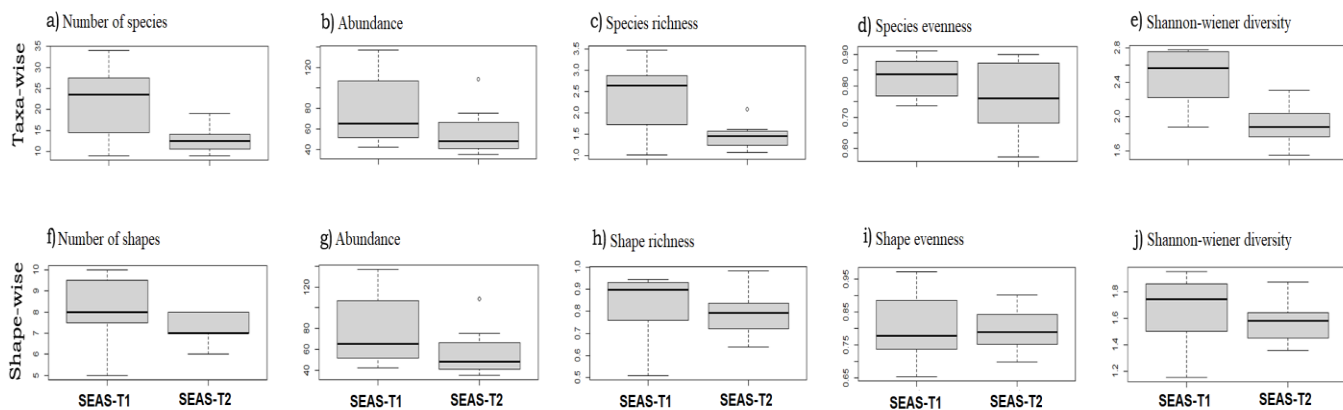
36.	<i>Lauderia sp.</i>	0	76	0	
37.	<i>Leptocylindrus sp</i>	22	2958	4	
38.	<i>Melosira sp</i>	6	0	0	
39.	<i>Planktonella sol</i>	56	0	11	
40.	<i>Rhizosolenia alata</i>	1220	6	78	
41.	<i>Rhizosolenia bergonii</i>	411	2	37	
42.	<i>Rhizosolenia calcar-avis</i>	351	3	27	
43.	<i>Rhizosolenia castracanei</i>	6	0	0	
44.	<i>Rhizosolenia hebetata</i>	479	9	5	
45.	<i>Rhizosolenia imbricata</i>	55	97	18	
46.	<i>Rhizosolenia robusta</i>	10	0	0	
47.	<i>Rhizosolenia setigera</i>	309	969	13	
48.	<i>Rhizosolenia sp</i>	34	0	4	
49.	<i>Rhizosolenia stolterfothii</i>	84	0	0	
50.	<i>Rhizosolenia styliformis</i>	1509	15	18	
51.	<i>Thalassiosira sp</i>	691	2823	236	
52.	<i>Corethron sp</i>	5	13	0	Cylinder + 2
53.	<i>Skeletonema sp</i>	548	34126	0	Half sphere (8)
54.	<i>Amphora sp</i>	1	82	0	Cymbelloid (9)
55.	<i>Hemidiscus sp</i>	19	0	0	
56.	<i>Alexandrium sp</i>	9	7	0	
57.	<i>Amphidinium sp</i>	10	0	0	
58.	<i>Ceratoperidinium sp</i>	58	0	0	
59.	<i>Dinophysis acuminata</i>	0	2	3	
60.	<i>Dinophysis caudata</i>	0	0	13	
61.	<i>Dinophysis miles</i>	0	4	0	
62.	<i>Dinophysis sp</i>	85	3	15	
63.	Diplonies sp	22	8	0	
64.	<i>Dissodinium bicorne</i>	2	0	0	
65.	<i>Dissodinium elegans</i>	46	0	0	
66.	<i>Dissodinium sp.</i>	0	1	0	
67.	<i>Gymnodinium sp</i>	14	51	98	
68.	<i>Gyrodinium sp</i>	127	162	230	
69.	<i>Karlodinium sp</i>	0	4	0	Ellipsoid (10)
70.	<i>Prorocentrum compressum</i>	0	0	2	
71.	<i>Prorocentrum dentatum</i>	0	26	55	
72.	<i>Prorocentrum gracile</i>	1	7	23	
73.	<i>Prorocentrum micans</i>	8	148	33	
74.	<i>Prorocentrum sp</i>	43	103	95	
75.	<i>Pyrocystis fusiformis f. fusiformis</i>	6	0	2	
76.	<i>Pyrocystis bamulum</i>	41	0	0	
77.	<i>Pyrocystis fusiformis f. lanceolata</i>	25	0	0	
78.	<i>Pyrocystis sp</i>	67	2	0	
79.	<i>Pyrophacus sp</i>	9	1	2	
80.	<i>Scrippsiella sp</i>	147	123	142	
81.	<i>Sinophysis sp.</i>	38	0	6	

82.	<i>Tripes biceps</i>	1	1	2	
83.	<i>Tripes azoricum</i>	1	0	0	
84.	<i>Tripes boehmii</i>	1	18	0	
85.	<i>Tripes borridum</i>	2	0	0	
86.	<i>Tripes breve var breve</i>	0	0	6	
87.	<i>Tripes breve var pulchellum</i>	0	0	4	
88.	<i>Tripes bumile</i>	0	0	4	
89.	<i>Tripes candelabrum var. candilabrum</i>	3	0	2	
90.	<i>Tripes contrarium</i>	2	0	0	
91.	<i>Tripes declinatum var angusiicorrum</i>	1	0	0	
92.	<i>Tripes declinatum var declinatum</i>	0	0	11	
93.	<i>Tripes deflexum</i>	0	2	8	
94.	<i>Tripes eherentbergii</i>	3	0	0	
95.	<i>Tripes extensum</i>	5	0	0	
96.	<i>Tripes furca var. berghii</i>	11	53	50	
97.	<i>Tripes furca var. eugrammum</i>	31	12	0	
98.	<i>Tripes fusus</i>	8	8	31	
99.	<i>Tripes fusus var. fusus</i>	5	0	0	
100.	<i>Tripes fusus var. schucttii</i>	3	0	0	Ellipsoid+2
101.	<i>Tripes gravidum</i>	1	0	0	Cone+ Cylinder
102.	<i>Tripes humile</i>	2	0	0	(11)
103.	<i>Tripes lineatum</i>	0	1	2	
104.	<i>Tripes longirostrum</i>	2	0	0	
105.	<i>Tripes longissimum</i>	1	0	0	
106.	<i>Tripes lunula var. lunula</i>	2	0	0	
107.	<i>Tripes macroceros var. gallicum</i>	0	0	8	
108.	<i>Tripes massiliense var. massiliense</i>	1	0	0	
109.	<i>Tripes pentagonum var. subrobustum</i>	4	0	0	
110.	<i>Tripes pentagonum var. tenerum</i>	6	37	4	
111.	<i>Tripes petersi</i>	0	0	6	
112.	<i>Tripes ramipes var. palmatum</i>	4	0	0	
113.	<i>Tripes sp</i>	64	1	0	
114.	<i>Tripes symmetricum var. coaractatum</i>	3	0	0	
115.	<i>Tripes teres</i>	20	2	0	
116.	<i>Tripes trichoceros</i>	62	0	0	
117.	<i>Tripes tripes var. atlanticum</i>	63	0	51	
118.	<i>Tripes tripes var. indicum</i>	0	0	2	
119.	<i>Tripes tripes var. pulchellum</i>	124	0	8	
120.	<i>Tripes vultur var japonicum</i>	1	0	0	
121.	<i>Amphiprora sp.</i>	1	13	0	
122.	<i>Chaetoceros atlanticum</i>	35	2	0	Elliptic prism
123.	<i>Chaetoceros coaractatus</i>	43	0	0	(12)
124.	<i>Chaetoceros laciniosus</i>	23	0	0	

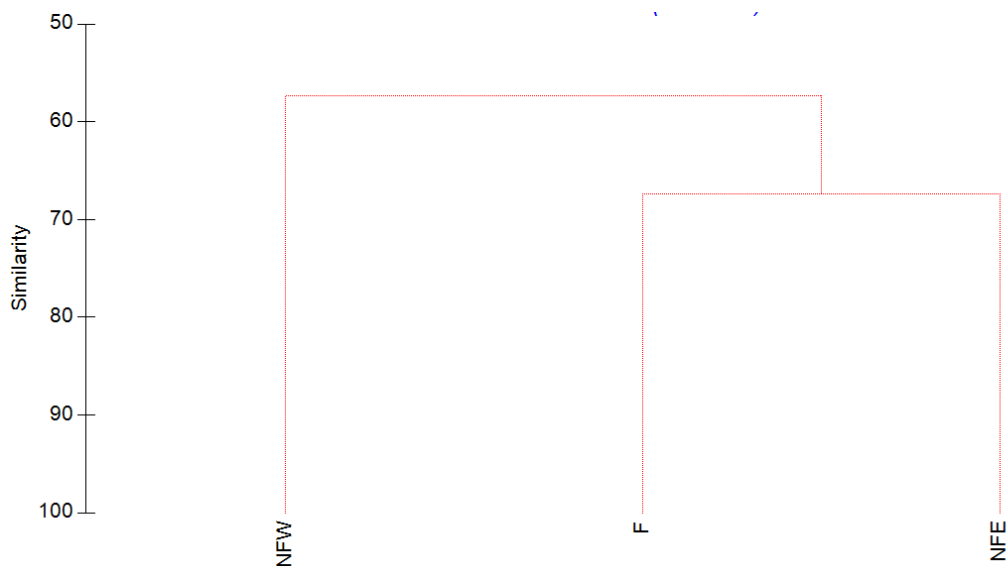
125.	<i>Chaetoceros peruvianus</i>	0	0	7	
126.	<i>Chaetoceros sp</i>	273	6125	487	
127.	<i>Eucampia sp</i>	1	23	0	
128.	<i>Fragilaria sp</i>	222	3	15	
129.	<i>Hemiaulus hauckii</i>	0	36	0	
130.	<i>Hemiaulus membranaceae</i>	0	44	0	
131.	<i>Hemiaulus sp</i>	122	6	0	
132.	<i>Meuneria sp</i>	186	14	0	
133.	<i>Navicula sp</i>	501	1146	483	
134.	<i>Navicula transistans</i>	39	0	0	
135.	<i>Odonetella mobilensis</i>	0	34	2	
136.	<i>Odontella sinensis</i>	0	1	0	
137.	<i>Odontella sp</i>	45	4	3	
138.	<i>Surirella sp</i>	36	0	0	
139.	<i>Trachyneis aspera</i>	2	0	0	
140.	<i>Climacodium sp</i>	431	31	47	Elliptic prism+ 4 Cones (13)
141.	<i>Ceratocorys armata</i>	1	0	0	
142.	<i>Ceratocorys sp</i>	17	0	4	Half sphere (14)
143.	<i>Ornithocercus sp</i>	139	0	5	
144.	<i>Nitzschia sp</i>	34	102	14	Prism on parallelogram (15)
145.	<i>Pleurosigma sp</i>	70	160	16	
146.	<i>Pseudonitzschia sp</i>	158	7529	1180	
147.	<i>Ditylum sp</i>	0	97	0	Prism on triangle (16)
148.	<i>Triceratium sp</i>	4	0	5	
149.	<i>Oxytoxum caudatum</i>	6	0	0	
150.	<i>Oxytoxum cf. crassum</i>	2	2	0	
151.	<i>Oxytoxum cf. globosum</i>	1	2	0	
152.	<i>Oxytoxum challengeroides</i>	1	0	0	
153.	<i>Oxytoxum curvatum</i>	1	13	0	
154.	<i>Oxytoxum curvicaudatum</i>	20	2	0	
155.	<i>Oxytoxum diploconus</i>	6	0	3	Prolated spheroid (17)
156.	<i>Oxytoxum lanticeps</i>	3	0	0	
157.	<i>Oxytoxum longum</i>	21	0	0	
158.	<i>Oxytoxum parvum</i>	0	0	4	
159.	<i>Oxytoxum scolopax</i>	17	6	12	
160.	<i>Oxytoxum sp</i>	43	27	3	
161.	<i>Oxytoxum tessellatum</i>	21	4	3	
162.	<i>Cylindrotheca closterium</i>	13	657	30	Prolated spheroid + 2 Cylinders (18)
163.	<i>Cladopyxis sp</i>	1	0	0	
164.	<i>Noctiluca sp</i>	169	1	0	Sphere (19)
Total		12606	64204	5541	



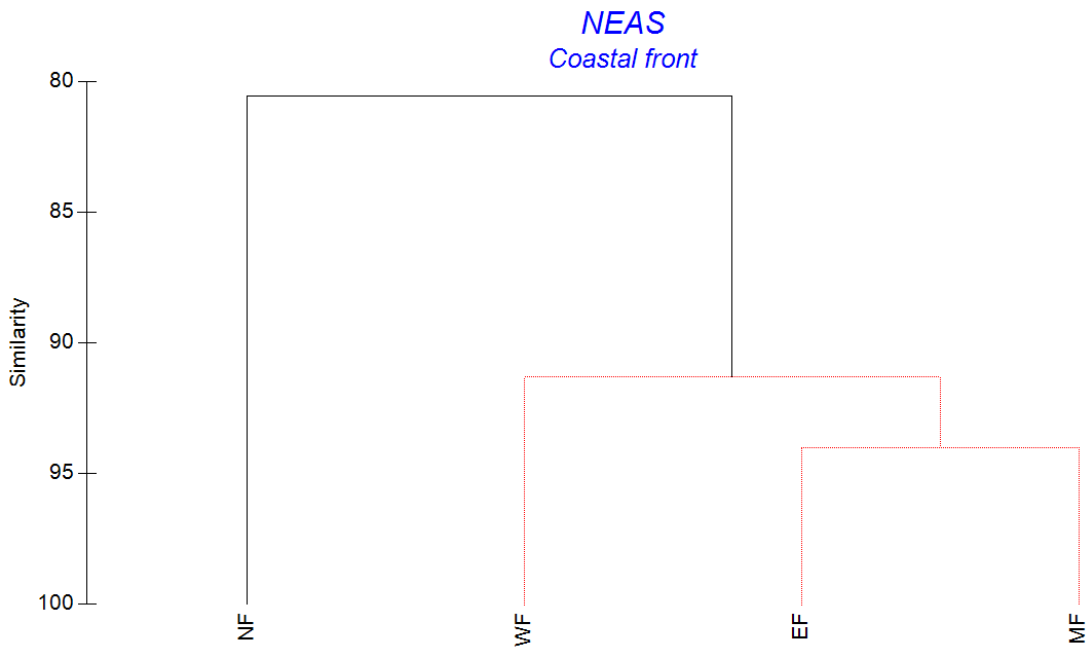
Supplementary Fig. 1. Map showing Sea level anomaly (SLA) plot with SST frontal and non-frontal regions in coastal region of NEAS. The blue line is showing the location of the fronts, the black rectangle and white oval shapes showing the frontal and non-frontal part sampled in the present study.



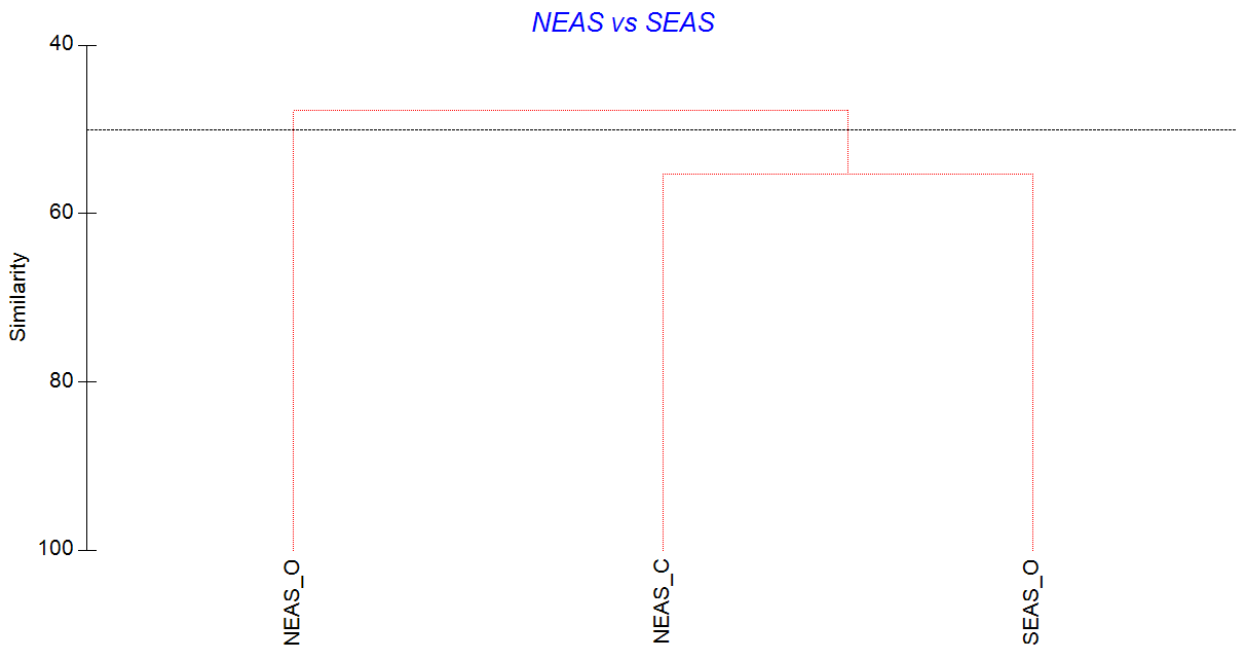
Supplementary Fig. 2. Univariate measures of phytoplankton (both taxonomy and shape-wise) from transects T1 and T2 of SEAS (open ocean). Station data are pooled and presented here.



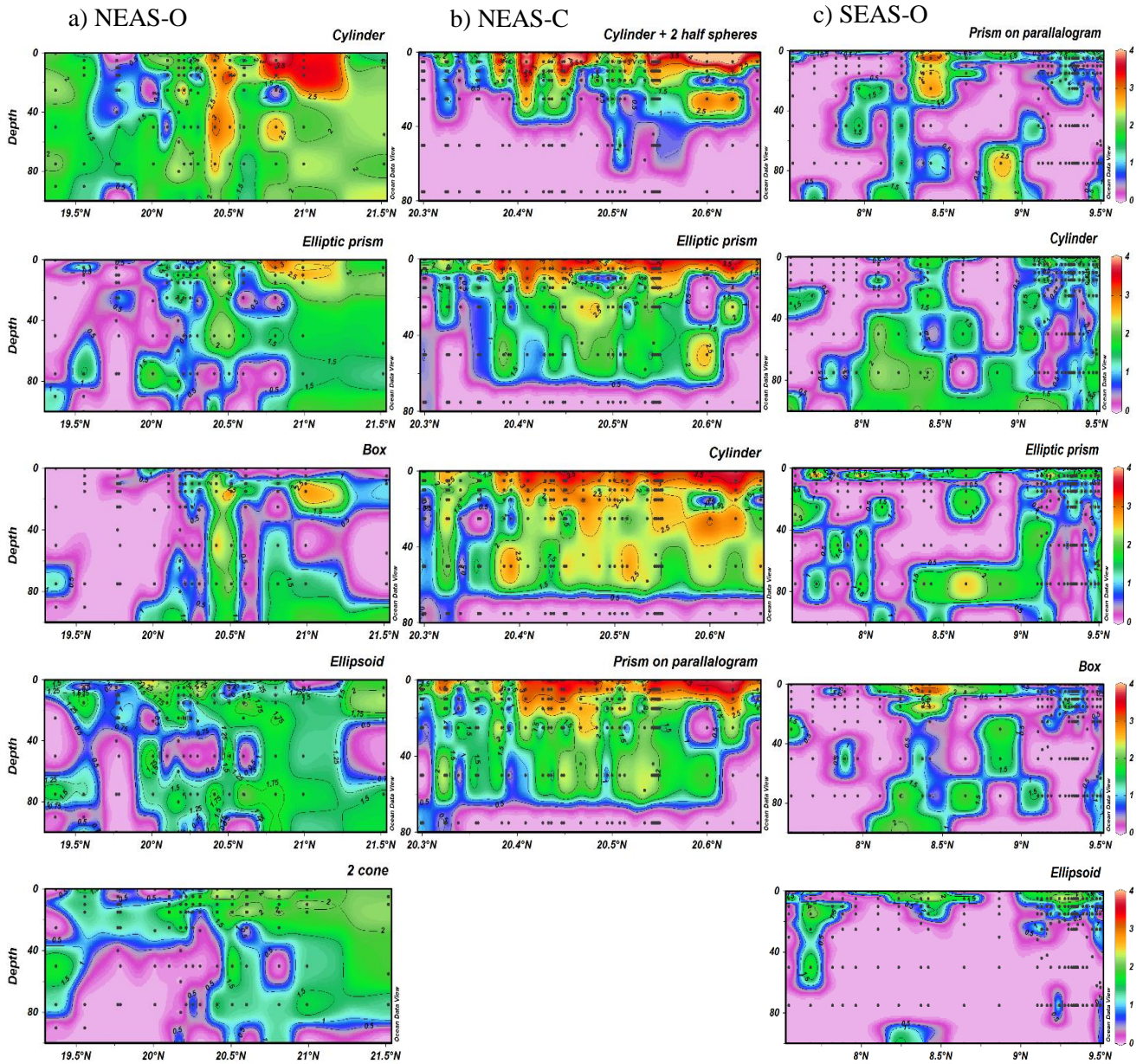
Supplementary Fig. 3. Taxonomy wise Cluster plot of open ocean frontal and non-frontal region micro-phytoplankton community of SEAS. NFW: Non-front West, F: Frontal region and NFE: Non-front East.



Supplementary Fig. 4. Shape-wise cluster plot of micro-phytoplankton community of frontal and non-frontal coastal NEAS. WF: West front, EF: East front, MF: Main front and NF: Non-front.



Supplementary Fig. 5. Taxonomy wise cluster plot of micro-phytoplankton community of NEAS and SEAS. NEAS-O: North-eastern Arabian Sea open ocean, NEAS-C: North-eastern Arabian Sea coastal region and SEAS-O: South-eastern Arabian Sea open ocean.



Supplementary Fig. 6. Distribution of dominant phytoplankton shape in the water column of NEAS and SEAS. NEAS-O: North-eastern Arabian Sea open ocean; NEAS-C: North-eastern Arabian Sea coastal region and SEAS-O: South-eastern Arabian Sea open ocean.